Diurnal variations in oxygen and nitrogen isotopes of atmospheric nitrogen dioxide and nitrate: implications for tracing NOx oxidation pathways and emission sources

Sarah Albertin, Joël Savarino, Slimane Bekki, Albane Barbero, Roberto Grilli, Quentin Fournier, Irène Ventrillard, Nicolas Caillon, Kathy S. Law

https://doi.org/10.5194/egusphere-2023-744
Preprint. Discussion started: 28 April 2023

Diurnal variations in oxygen and nitrogen isotopes of atmospheric nitrogen dioxide and nitrate: implications for tracing NO_x oxidation pathways and emission sources

Sarah Albertin[1,2], Joël Savarino[2], Slimane Bekki[1], Albane Barbero[2], Roberto Grilli[2], Quentin Fournier[3], Irène Ventrillard[3], Nicolas Caillon[2], Kathy Law[1]

[1]LATMOS/IPSL, Sorbonne Université, UVSQ, CNRS, 75005 Paris, France.
[2]IGE, Univ. Grenoble Alpes, CNRS, IRD, Grenoble INP, 38000 Grenoble, France.
[3]LIPhy, Univ. Grenoble Alpes, CNRS, 38000 Grenoble, France.

Correspondence to: Sarah Albertin (sarah.albertin@univ-grenoble-alpes.fr)

Abstract. The oxygen ($\Delta^{17}O$) and nitrogen ($\delta^{15}N$) isotopic compositions of atmospheric nitrate (NO_3^-) are widely used as tracers of its formation pathways, precursor (nitrogen oxides NO_x = nitric oxide NO + nitrogen NO_2) emission sources, and physico-chemical processing. However, the critical lack of observations on the multi-isotopic composition of NO_2 maintains significant uncertainties regarding the links between the isotopic composition of NO_x and NO_3^-, which may bias estimates of the NO_3^- formation processes and the distribution of sources. We report here on the first simultaneous atmospheric observations of $\Delta^{17}O$ and $\delta^{15}N$ in NO_2 and NO_3^-. The measurements were carried out at sub-daily (~ 3 h) resolution over two non-consecutive days in an Alpine city in February 2021. Important diurnal variabilities are observed in both NO_2 and NO_3^- multi-isotopic composition. $\Delta^{17}O$ of NO_2 and NO_3^- ranges from 19.6 to 40.8 ‰ and 18.7 to 26 ‰, respectively. During the day and night, the variability of $\Delta^{17}O(NO_2)$ is mainly driven by the oxidation of NO by ozone, with a substantial contribution from peroxy radicals in the morning. NO_3^- local mass balance equations, constrained by observed $\Delta^{17}O(NO_2)$, suggest that during the first day of sampling, NO_3^- was formed locally from the oxidation of NO_2 by hydroxyl radicals during the day, and via heterogeneous hydrolysis of dinitrogen pentoxide during the night. For the second day, calculated and observed $\Delta^{17}O(NO_3^-)$ do not match, particularly daytime values. The effects on $\Delta^{17}O(NO_3^-)$ of a Saharan dust event that occurred during the second day and winter boundary layer dynamics are discussed. $\delta^{15}N$ of NO_2 and NO_3^- ranges from −10.0 to 19.7 ‰ and −4.2 to 14.8 ‰, respectively. Consistent with theoretical predictions of N isotope fractionation, the important variability of $\delta^{15}N(NO_2)$ is explained by significant post-emission equilibrium N fractionation. After accounting for this effect, vehicle exhaust is found to be the primary source of NO_x emissions at the sampling site. $\delta^{15}N(NO_3^-)$ is closely linked to $\delta^{15}N(NO_2)$ variability, which bring further evidence of fast and local processing, but uncertainties on current N fractionation factors during NO_2 to NO_3^- conversion are underscored. Overall, this detailed investigation highlights the potential and the necessity to use $\Delta^{17}O$ and $\delta^{15}N$ in NO_2 and NO_3^- to trace quantitatively the sources and formation chemistry of NO_3^-, particularly in urban environments in winter.

https://doi.org/10.5194/egusphere-2023-744
Preprint. Discussion started: 28 April 2023

1 Introduction

Despite emission control efforts since the last decades, global anthropogenic emissions of nitrogen oxides (NO_x = nitrogen monoxide NO + nitrogen dioxide NO_2) remain more than two orders of magnitude higher than before the Industrial Revolution (Hoesly et al., 2018). NO_x chemistry is closely linked with the atmosphere's oxidative capacity (i.e. the ability of the atmosphere to oxidise and remove trace gases including pollutants), notably through their influence on the production of ozone (O_3) and hydroxyl radical (OH) (Finlayson-Pitts and Pitts, 2000). NO_x are mainly oxidized into atmospheric inorganic nitrate (NO_3^- = nitric acid HNO_3 + particulate nitrate p-NO_3^-), which can be transported far from emission sources and be removed from the atmosphere through dry and wet deposition, within hours to days (Alexander et al., 2020; Park et al., 2004). The additional input of this so-called "reactive" nitrogen (N_r) into natural environments is known to have harmful consequences, particularly on biodiversity and water quality (Galloway et al., 2008; Vitousek et al., 1997). NO_3^- is also a key component of fine particulate matter (PM) with adverse effects on health (WHO, 2021) and on the climate (IPCC, 2021). Various factors can influence the NO_3^- content in PM, including precursor emission sources, complex multiphase chemical reactions with other species, and environmental conditions (temperature, relative humidity, solar radiation) (Zhang et al., 2015). It is therefore important to have a comprehensive understanding of the global and local parameters that contribute to the production of NO_3^-, on which effective mitigation strategies for air quality and climate change rely (e.g., Bauer et al., 2007; Huang et al., 2014; Shah et al., 2018; Tsimpidi et al., 2008; Wang et al., 2013, 2020).

NO_x is mainly emitted as NO, which, upon release into the atmosphere, undergoes oxidation to form NO_2. During the day, a rapid photochemical equilibrium is established between NO and NO_2, known as the "photostationary state" (PSS; Leighton, 1961 citation), via key interconversion reactions:

$$NO_2 + h\nu \xrightarrow{M} O(^3P) + NO \quad \text{R1}$$

$$O(^3P) + O_2 \xrightarrow{M} O_3 \text{ with } M = N_2 \text{ or } O_2 \quad \text{R2}$$

$$NO + O_3 \rightarrow NO_2 + O_2 \quad \text{R3}$$

This cycle can be disturbed by peroxy radicals (RO_2 = hydroperoxyl radical HO_2 + methyl peroxy radical CH_3O_2) leading to the formation of O_3 (Crutzen, 1979):

$$NO + RO_2 \rightarrow NO_2 + RO \quad \text{R4}$$

During the daytime, the homogeneous reaction of NO_2 with OH is the most important loss mechanism for NO_x (Dentener and Crutzen, 1993):

$$NO_2 + OH \xrightarrow{M} HNO_3(g) \quad \text{R5}$$

https://doi.org/10.5194/egusphere-2023-744
Preprint. Discussion started: 28 April 2023

NO_2 can also react with O_3 to form NO_3 radicals (Reaction R6):

$$NO_2 + O_3 \xrightarrow{M} NO_3 + O_2 \quad \text{R6}$$

However, NO_3 is rapidly photolyzed during the day regenerating back NO_2 (Wayne et al., 1991). Another important NO_3 loss reaction, is that with NO in polluted environments (Brown and Stutz, 2012). At night, without photolytic activity, the lifetime of NO_3 radicals can substantially increase. Therefore, NO_3 reacts with NO_2 to form dinitrogen pentoxide (N_2O_5; Reaction R7), which then undergoes heterogeneous hydrolysis to form HNO_3 (Reaction R8):

$$NO_3 + NO_2 \overset{M}{\leftrightarrow} N_2O_5 \quad \text{R7}$$

$$N_2O_5 + H_2O(\text{aerosol}) \rightarrow 2\,HNO_3(aq) \quad \text{R8}$$

N_2O_5 is an important nocturnal sink for NO_x, but Reaction R7 is temperature dependent, so it can eventually decompose to reform NO_2 and NO_3. The lowest temperatures promote the stability of N_2O_5. However, the yield of Reaction R8 remains uncertain as it strongly depends on the aerosol surface density and its chemical composition (Brown, 2006). Globally, Reactions R1–R8 are estimated to lead to the formation of 82 % of NO_3^- near the surface (Alexander et al., 2020). However, other reactions such as through halogen and organic intermediates become more significant for NO_3^- production in specific regions of the world, like the polar, oceanic, and coastal areas (Alexander et al., 2020; Penkett et al., 2007; Savarino et al., 2013; Simpson et al., 2015). Although the main chemical processes involved in the production of NO_3^- have been identified, reaction yields, source of radical species (e.g., OH, RO_2), and relative contributions of each process in the formation of NO_3^- still remain a large area of uncertainty (Alexander et al., 2020; Brown, 2006; Newsome and Evans, 2017; Xue, 2022).

To better constrain the atmospheric N_r chemistry and budget, the last three decades have seen a growing interest in stable oxygen (O) and nitrogen (N) isotopes, notably through the use of ^{17}O anomalies ($\Delta^{17}O$) and ^{15}N enrichments ($\delta^{15}N$) in NO_3^- (Elliott et al., 2019; Savard et al., 2018). The isotopic composition is reported as an isotopic enrichment (δ) with respect to a reference material, defined as $\delta = (R_{sample}/R_{reference} - 1)$, and expressed in per mill (‰). R refers to the elemental abundance ratio of the heavy isotope to the light isotope (e.g., $^{18}O/^{16}O$; $^{17}O/^{16}O$; $^{15}N/^{14}N$) in the sample, and in an international isotopic reference material (Vienna Standard Mean Ocean Water for O; Li et al., 1988, and atmospheric N_2 for N; Mariotti, 1984).

The oxygen isotopic composition of NO_3^- is usually investigated in light of its ^{17}O-excess ($\Delta^{17}O = \delta^{17}O - 0.52 \times \delta^{18}O$). $\Delta^{17}O$ is primarily transferred by O_3 which possesses a very unique ^{17}O anomaly ((26 ± 2) ‰; Vicars and Savarino, 2014) due to mass-independent fractionation during its formation process (Thiemens, 2006). In comparison, the $\Delta^{17}O$ of other atmospheric oxidants such as OH is near zero due to isotopic exchange with atmospheric water vapor (Dubey et al., 1997). Similarly, as the isotopic anomaly of atmospheric O_2 is very close to 0 ‰ (Barkan and Luz, 2003), and since RO_2 are mostly produced

https://doi.org/10.5194/egusphere-2023-744
Preprint. Discussion started: 28 April 2023

reactions R + O_2 and H + O_2, $\Delta^{17}O$ of RO_2 can be considered negligible (Alexander et al., 2020). By a simple mass balance calculation of O atoms in NO_3^-, the ^{17}O anomaly of NO_3^- produced by each NO_2 to NO_3^- conversion formation process *i* ($(\Delta^{17}O(NO_3^-)_i)$) can be expressed as:

$$\Delta^{17}O(NO_3^-)_i = \frac{2}{3} \times \Delta^{17}O(NO_2) + \frac{1}{3} \times \Delta^{17}O(\text{add. O})_i \quad (1)$$

where $\Delta^{17}O(NO_2)$ is the ^{17}O-excess of atmospheric NO_2 and $\Delta^{17}O(\text{add. O})_i$ is the transferrable ^{17}O-excess of the oxidant responsible for the conversion of NO_2 in NO_3^- (Michalski et al., 2003). Therefore, $\Delta^{17}O$ in NO_3^- represents a unique tracer of the N_r chemistry, that can provide valuable constraints on the relative contributions of individual reactions (Morin et al. 2011, Alexander et al., 2009; Michalski et al., 2003). $\Delta^{17}O(NO_3^-)$ has been initially measured in polar regions to extract information on NO_3^- chemistry and on the past AOC from NO_3^- archived in ice cores (e.g., Alexander et al., 2004; McCabe et al., 2007; Morin et al., 2008; Savarino et al., 2016; Geng et al., 2017). More recent studies in urban areas have attempted to interpret the variability of $\Delta^{17}O(NO_3^-)$ in aerosols in order to quantify the relative contribution of homogeneous and heterogeneous processes in the formation of NO_3^- (Fan et al., 2023, 2022; He et al., 2020, 2018; Li et al., 2022b; Lim et al., 2022; Wang et al., 2023, 2019; Zhang et al., 2022b).

Although $\Delta^{17}O(NO_3^-)$ records can be a valuable asset in improving the understanding of NO_3^- chemistry in urban areas, Eq. (1) shows clearly that, in order to interpret $\Delta^{17}O(NO_3^-)$ observations in term of oxidation processes, the value of $\Delta^{17}O(NO_2)$ must be constrained. However, to date there is a lack of observational data to accurately determine the behaviour of $\Delta^{17}O(NO_2)$, which is thought to be highly variable in polluted regions (Albertin et al., 2021; Michalski et al., 2014). Most studies typically estimate $\Delta^{17}O(NO_2)$ during the day by assuming that an isotopic steady state is reached between NO_x and O_3. Likewise, during the night they assume that the isotopic composition of NO_2 reflects the daytime conditions of the preceding days, as the nighttime oxidation of NO_2 into NO_3^- exceeds the duration of the night (Alexander et al., 2020). Even though this assumption may hold true in remote areas, significant uncertainties persist in urban areas where nocturnal NO_3^- chemistry can be more efficient. In a recent study in urban Grenoble, France, the first *in situ* observations of $\Delta^{17}O(NO_2)$ showed important diurnal variability (Albertin et al., 2021), largely influenced by local environmental conditions. Authors highlighted the importance to provide additional observational data on the dynamics of $\Delta^{17}O(NO_2)$, and its links with $\Delta^{17}O(NO_3^-)$ to accurately interpret observations of $\Delta^{17}O(NO_3^-)$ in urban areas, particularly at sub-daily time scales.

$\delta^{15}N$ in NO_3^- ($\delta^{15}N(NO_3^-)$) can be used as a tracer of NO_3^-sources and/or chemical processing. On the one hand, as NO_x emissions have a distinct $\delta^{15}N$-fingerprint that depends on the production mechanism (Heaton, 1990; Felix et al., 2012; Fibiger and Hastings, 2016; Walters et al., 2015a, b; Yu and Elliott, 2017; Miller et al., 2018), $\delta^{15}N(NO_3^-)$ is a potentially valuable tool for tracing the origin of its gaseous precursor. However, due to N fractionation effects during physico-chemical processing, $\delta^{15}N$ can be altered during the conversion of NO_x into NO_3^- (Elliott et al., 2019). Therefore, the variability of

https://doi.org/10.5194/egusphere-2023-744
Preprint. Discussion started: 28 April 2023

$\delta^{15}N(NO_3^-)$ can be attributed to: (1) a change in NO_x emission sources and (2) N isotopic fractionations between NO and NO_2, and/or between NO_2 and NO_3^-, and/or during the transport of NO_3^- in the atmosphere. Both of these effects are likely to coexist, and their relative influence can vary depending on the environmental conditions. Fluctuations in $\delta^{15}N(NO_3^-)$ have been directly interpreted as a change in NO_x emissions sources (Altieri et al., 2022; Elliott et al., 2007; Hastings et al., 2009), which seemingly ignore the potential impact of post-emission fractionation. However, numerous observations in diverse environments have emphasized the substantial influence of N fractionation effects in altering the original ^{15}N composition of gaseous NO_3^- precursors (e.g., Bekker et al., 2023; Chang et al., 2018; Geng et al., 2014; Li et al., 2021; Luo et al., 2023; Vicars et al., 2013). Although some N fractionation factors are available from calculations (Walters and Michalski, 2015) and laboratory experiments (Li et al., 2020; Walters et al., 2016), there is still a lack of observational constraints on the magnitude of the N isotopic partitioning between NO_x and NO_3^-, which could lead to biased interpretations of the $\delta^{15}N(NO_3^-)$ observations, and hamper a quantitative apportionment of NO_x emission sources.

In the continuity of the preliminary work investigated by Albertin et al. (2021), this study presents for the first time the simultaneous measurements of the atmospheric NO_2 and NO_3^- multi-isotopic compositions at high temporal resolution (~ 3 h) in late February 2021 in an urban Alpine city. On the one hand, the added value of the NO_2 multi-isotopic composition measurements is further assessed than in Albertin et al. (2021) through the use of more accurate measurements of NO and NO_2 mixing ratios. Sub-daily N_r chemistry and N fractionation effects are investigated by collating $\Delta^{17}O/\delta^{15}N$ data, meteorological parameters, and atmospheric observations (NO, NO_2, O_3 and PM). On the other hand, using the isotopic theoretical framework applied in previous research, we explore the potential benefits of combining isotopic observations of NO_2 and NO_3^- to gain a more detailed understanding on the links between atmospheric N_r chemistry processes and variability in NO_2 and NO_3^- isotopic composition. This first study case of the concurrent multi-isotopic composition of NO_2 and NO_3^- was carried out with the aim of developing more quantitative isotopic tools for tracing the origin and fate of NO_x, in particular for urban regions on a sub-daily time scale.

2 Material and methods

2.1 Study site and sample collection

The study was conduction in February 2021 in Chamonix-Mont-Blanc, France, (45°55′21″ N, 6°52′11″; altitude 1035 m above sea level (m.a.s.l)). This narrow (~2 km wide on average in Chamonix) 23 km Alpine valley of about 12,000 inhabitants is surrounded by high-elevation mountains. The city can experience severe PM pollution events during the winter season, mainly due to wood-combustion for domestic heating and road traffic (Chazette et al., 2005; Quimbayo-Duarte et al., 2021; Weber et al., 2018; Aymoz et al., 2007). The study's sampling site was located at a CNRS (Centre National de la Recherche Scientifique) facility in a residential area, 1.2 km south of the Chamonix city centre, and 1.4 km north of the

https://doi.org/10.5194/egusphere-2023-744
Preprint. Discussion started: 28 April 2023

Mont-Blanc tunnel. Ambient air monitoring inlets and off-line gas and aerosol samplers were installed on the facility's terrace, 3 m above the ground level (m.a.g.l). Over the campaign, the surface was partly covered with snow.

Atmospheric particles (aerosols) were collected using a high-volume sampler (Digitel®, DH77, TSP inlet, 1 m^3 min^{-1}) and glass microfiber filters (Whatman®, 150 mm-diameter) that quantitatively collect total NO_3^- (Morin et al., 2007; Frey et al., 2009; Erbland et al., 2013). Concurrently, atmospheric NO_2 was collected using a pre-cleaned honeycomb denuder tube coated with a mixture of 2.5 M KOH (in methanol) and ultrapure guaiacol inserted into a ChemComb® 3500 speciation cartridge (Thermo Scientific®, USA). A second coated denuder was placed in series into the cartridge to check for NO_2 breakthrough. After sampling, denuders were rinsed with 10 mL of deionized water to solubilized trapped NO_2. Denuder extractions and atmospheric filters were stored and transported frozen until analysis at the IGE (Grenoble, France). Detailed information on the sampling protocol is available in Albertin et al. (2021).

Following the objective to investigate the diurnal isotopic composition of NO_2 and NO_3^-, denuder and filter samplings were conducted continuously for 24 hours with sampling time steps ranging from 1h30 to 7h30. During the day, denuder and filter samplings were synchronized. At night, two filter samplings were performed while three sets of denuder tubes were collected. This sampling protocol was conducted during two non-consecutive days, from 19 February 2021 21:00 local time (LT) to 20 February 2021 21:00 LT (sampling period #1 = SP 1) and from 24 February 2021 7:30 LT to 25 February 2021 7:30 LT (sampling period #2 = SP 2).

2.2 Chemical and isotopic analysis

Concentrations of major ions from filter samples were determined by ion chromatography (Thermo Scientific™ Dionex™ Integrion™ HPIC) and corrected by the arithmetic mean of the concentrations measured on the field blanks, representing on average (8 ± 9) %. Atmospheric mass concentrations (expressed in μg m^{-3}) were calculated as the ratio of the total ion filter loading to the total volume of air pumped through the filter at STP conditions. NO_2^- concentration in denuder extractions were first estimated using the Griess-Saltzmann reaction and UV–Vis spectrometry at 544 nm. Even though the eluted matrix can interfere with colorimetric analyses, measured concentrations on first denuder tubes were relatively well correlated with ambient NO_2 measurements during atmospheric sampling and allowed to give indications on field blanks and on the volume needed to perform isotopic analysis.

Isotopic analyses were performed using an isotope ratio mass spectrometer (IRMS, Thermo Finnigan™ MAT 253) for analyses of $^{15}N/^{14}N$, $^{17}O/^{16}O$, and $^{18}O/^{16}O$ in NO_3^- and NO_2 samples. Briefly, NO_3^- from filter extractions were converted into gaseous N_2O by the bacterial denitrifier method (Sigman et al., 2001; Casciotti et al., 2002; Kaiser et al., 2007) in which ≈100 nmol of NO_3^- ions were injected into a 2 mL of a bacteria medium (strain of *Pseudomonas aureofaciens*) under anaerobic conditions. NO_2 denuder extractions were treated with the azide method (McIlvin and Altabet, 2005; Albertin et al., 2021) in which 2 mL of a sodium azide 2M /acetic acid 100 % buffer were injected into ≈100 nmol of NO_2^- allowing quantitative conversion into N_2O. For both type of extractions, once ions were converted into N_2O, the latter was thermally

https://doi.org/10.5194/egusphere-2023-744
Preprint. Discussion started: 28 April 2023

decomposed into O_2 and N_2 in a gold tube heated at 850 °C. O_2 and N_2 molecules were then separated on a chromatography column and sent separately into the IRMS for the dual analysis of O and N isotopes (see Morin et al., 2009 for more details on the analytical line).

Possible isotopic changes resulting from the conversion and analysis process of NO_3^- and NO_2^- ions were evaluated using international isotopic reference materials (Table S4 in the Supplement). Accuracy of the analytical method was estimated as the standard deviation (σ) of the residuals between measurements of the reference materials and their expected values. In our study, average measurement uncertainties on $\delta^{15}N$, $\delta^{17}O$, $\delta^{18}O$, and $\Delta^{17}O$ were estimated to be ±0.3 ‰, ±0.9 ‰, ±1.3 ‰, and ±0.4 ‰, respectively, for NO_3^- samples and ±0.3 ‰, ±0.4 ‰, ±0.9 ‰, and ±0.3 ‰, respectively, for NO_2 samples. Detailed information about the calibration procedure can be found in Morin et al. (2009) for NO_3^- and in Albertin et al. (2021) for NO_2^-.

Each NO_3^- sample was analysed in triplicate (the mean value of replicate measurements and the associated repeatability are reported in Table S3 in the Supplement). The limited amount of NO_2 samples did not allow for replicate measurements. All NO_2 samples presented a negligible blank (< 4%; mean of 1.7 nmol ml^{-1}) except for the sample collected between 13:30 and 16:30 LT during SP 2 which show a blank around (14.0 ± 1.4) %. Therefore, the measured $\Delta^{17}O$ of this sample was corrected for blank effect assuming that the contaminated NO_2^- possessed a $\Delta^{17}O$ = 0 ‰. No correction from this blank effect was applied on the $\delta^{15}N$ measurements of NO_2 because the $\delta^{15}N$ fingerprint of the contamination could not be characterized. This uncertainty is propagated in the calculations of section 4 and considered in the discussions.

2.3 Ancillary data

During atmospheric samplings, surface NO_x mixing ratios were measured at the study site using an incoherent broadband cavity-enhanced absorption spectrometer for NO_2 (IBBCEAS; Barbero et al., 2020) and an optical-feedback cavity-enhanced absorption spectrometer for NO (OFCEAS; Richard et al., 2018). PM concentrations (PM_{10} and $PM_{2.5}$) were monitored by an optical particle counter (GRIMM®, EDM 164). O_3 mixing ratio was monitored at the local air quality monitoring site located a kilometre north of the sampling site (Environnement SA®, O3 42M; https://www.atmo-auvergnerhonealpes.fr/, last access: 5 November 2021).

Surface temperature ($T_{surface}$) and relative humidity (RH) were measured by a portable logger (Tinytag, TGP-4500, Gemini Data Loggers) located at the air quality monitoring site. Vertical temperatures were measured from 11 similar loggers fixed along the Plan-Praz cable car (45°55′39″ N, 6°51′55″ E) from 1098 to 2021 m.a.s.l. (data obtained from personal communications with C. Coulaud, IGE).

The NO_2 photolysis rate (J_{NO_2}) was calculated for the two sampling periods using a photochemical boxmodel (CiTTyCAT version 2.02; Galeazzo et al., 2018; Pugh et al., 2012) using the Fast-J photolysis scheme of Wild et al. (2000) and a surface albedo fixed to 0.65, a value representative of a snow-covered surface (average value between fresh and old snow; more details can be found in Text S1 in the Supplement).

https://doi.org/10.5194/egusphere-2023-744
Preprint. Discussion started: 28 April 2023

2.4 Interpretation framework for isotopic signals

In this section, we briefly state the key concepts and equations necessary to interpret isotopic signals measured in NO_2 and NO_3^-. A more detailed description and complete equation derivations can be found in cited references.

2.4.1 $\Delta^{17}O$ mass balance equations

Considering the mass conservation of $\Delta^{17}O$ in the atmospheric Nr cycle, a general mass balance equation of $\Delta^{17}O$ in a species X can be established (in this study X = NO_2 or NO_3^-). As NO_2 and NO_3^- loss processes do not fractionate in terms of the oxygen mass-independent anomaly, an overall expression of the time derivative of $\Delta^{17}O$ in the species X ($\Delta^{17}O(X)$) is derived as a function of its deviation from $\Delta^{17}O$ transferred through each production channel i (P_i) ($\Delta^{17}O_i(X)$), weighted according to the relative contributions of the production channels (Vicars et al., 2013):

$$\frac{\mathrm{d}}{\mathrm{d}t}\left(\Delta^{17}\mathrm{O(X)}\right) = \frac{1}{\tau(X)} \times \sum_i \frac{P_i}{\sum_i P_i} \times \left(\Delta^{17}\mathrm{O}_i\mathrm{(X)} - \Delta^{17}\mathrm{O(X)}\right) \quad (2)$$

where P_i expresses reaction rate constant times the atmospheric concentrations of reacting species, and τ is the atmospheric lifetime of the species X at steady state ($\tau = [\mathrm{X}]/\sum_i P_i$ with [X] being the atmospheric mixing ratio of the species X).

During the day, the rapid photochemical cycling of NO_x (Reactions R1–R4) leads to an isotopic equilibrium between NO and NO_2, i.e. $\Delta^{17}O(NO) \approx \Delta^{17}O(NO_2)$ (Michalski et al., 2014). Therefore, using the steady state approximation, and considering Reactions NO + O_3 (R3) and NO + RO_2 (R4) as the main sources of NO_2 at our site, the overall daytime $\Delta^{17}O$ in NO_2 can be expressed by:

$$\Delta^{17}\mathrm{O}_{\mathrm{day}}(\mathrm{NO_2}) \approx T_{\mathrm{NO+O_3}} \times \Delta^{17}\mathrm{O}_{\mathrm{NO+O_3}}(\mathrm{NO_2}) \quad (3)$$

where $\Delta^{17}\mathrm{O}_{\mathrm{NO+O_3}}(\mathrm{NO_2})$ is the O_3 isotopic anomaly transferred to NO through NO + O_3 (R3) (Savarino et al., 2008).

$T_{\mathrm{NO+O_3}}$ represents the proportion of O atoms originating from O_3 in NO_2, and hence the relative importance of Reaction NO + O_3 (R3) in the conversion of NO into NO_2 (Michalski et al., 2003; Morin et al., 2007; Albertin et al., 2021):

$$T_{\mathrm{NO+O_3}} = \frac{k_{\mathrm{NO+O_3}}[\mathrm{O_3}]}{k_{\mathrm{NO+O_3}}[\mathrm{O_3}] + k_{\mathrm{NO+RO_2}}[\mathrm{RO_2}]} \quad (4)$$

where $k_{\mathrm{NO+O_3}}$ is the kinetic constant of Reaction R3 and $k_{\mathrm{NO+RO_2}}$ the kinetic constant of Reaction R4. The kinetic constants used in this study are listed in Table A1 in the Appendix.

At night, the lifetime of NO_2 relative to dry deposition and oxidation via O_3 is of the order of 10 h (Table B1). Considering that (1) $\Delta^{17}O(NO) \approx 0$ ‰ (NO_x emission without NO_2 recycling), (2) no $\Delta^{17}O$ equilibrium between NO and NO_2 (no

https://doi.org/10.5194/egusphere-2023-744
Preprint. Discussion started: 28 April 2023

photochemical cycling), and (3) O_3 is the main oxidant of NO (no nighttime production of RO_2), the overall $\Delta^{17}O(NO_2)$ at night is determined by the $\Delta^{17}O$ transfer via Reaction R3 and by the nighttime residuals of NO_2 formed during the previous daytime hours (Albertin et al., 2021):

$$\Delta^{17}O_{night}(NO_2) \approx x \times \Delta^{17}O_{day}(NO_2) + \frac{(1 - x)}{2} \times (\Delta^{17}O_{NO+O_3}(NO_2) + \Delta^{17}O(NO)) \quad (5)$$

where x is the fraction of NO_2 formed during the day to the total NO_2 measured at night.

At our sampling site, we hypothesize Reaction R5 (OH pathway) and Reactions R6–R8 (N_2O_5 pathway) as the main NO_3^- daytime and nighttime production channels, respectively. At steady state, we derive from Eq. (2) general daytime and nighttime expressions for $\Delta^{17}O$ in NO_3^- associated with the OH and N_2O_5 pathways, respectively:

$$\Delta^{17}O_{day}(NO_3^-) \approx \frac{2}{3} \times \Delta^{17}O(NO_2) \quad (6)$$

$$\Delta^{17}O_{night}(NO_3^-) \approx \frac{2}{3} \times \Delta^{17}O(NO_2) + \frac{1}{6} \times \Delta^{17}O_{NO_2+O_3}(NO_3) \quad (7)$$

where $\Delta^{17}O_{NO_2+O_3}(NO_3)$ is the anomaly transfer from O_3 to NO_3 during Reaction R6 (Berhanu et al., 2012).

Without wet scavenging, dry deposition is the main sink of NO_3^- (Park et al., 2004). Assuming a mean NO_3^- deposition velocity of 0.5 cm s^{-1} (mean value of the dry deposition velocities of HNO_3 and *p*-NO_3^-; Zhang et al., 2009), and considering mean daytime and nighttime boundary layer heights of 500 m.a.g.l and 100 m.a.g.l (estimations based on vertical temperature profiles; Fig. S2 in the Supplement), respectively, the estimated NO_3^- lifetime against dry deposition is approximately 28 hours during the day, and 6 hours at night (Table B1). Therefore, on a sub-daily time scale, the ^{17}O-excess in NO_3^- is likely to reflect a combination of daytime and nighttime production processes.

2.4.2 Nitrogen isotopic fractionation effects

Each source of NO_x generates a $\delta^{15}N$ fingerprint which varies depending on the emission process (temperature and pressure) and the type of fuel (e.g., coal, oil, gas) (Heaton, 1990; Felix et al., 2012; Fibiger and Hastings, 2016; Walters et al., 2015a, b; Yu and Elliott, 2017; Miller et al., 2018). The mean $\delta^{15}N$ of NO_x ($\delta^{15}N(NO_x)$) emitted in the atmosphere results from the sum of each NO_x emission $\delta^{15}N$ fingerprint weighted by their relative contribution to the total NO_x emissions. Once in the atmosphere, NO_x are subjected to oxidation processes and isotopic exchanges that alter the initial $\delta^{15}N$ signature of NO_x emissions. As a result, $\delta^{15}N$ in NO_2 and in NO_3^- is a complex function of both the $\delta^{15}N$ signature of NO_x emissions and N isotopic effects. These later can be categorized into three groups: (1) the equilibrium isotope effect (EIE), (2) the kinetic

https://doi.org/10.5194/egusphere-2023-744
Preprint. Discussion started: 28 April 2023

isotope effect (KIE), and (3) the photochemical isotope fractionation effect (PHIFE). The magnitude of these isotopic effects is quantified as ^{15}N enrichment factor (ε), which is defined as ($\alpha - 1$), where α represents the N isotopic fractionation factor. A general expression for $\delta^{15}N(NO_2)$ can be derived as a function of a factor F_N which represents the overall N isotopic fractionation effects between NO_x and NO_2 (expressed in ‰), of the fraction of NO_x in the form of NO_2 (f_{NO_2} = [NO_2] / [NO_x]), and of $\delta^{15}N(NO_x)$ (Albertin et al., 2021):

$$\delta^{15}N(NO_2) = F_N \times (1 - f_{NO_2}) + \delta^{15}N(NO_x) \quad (8)$$

Therefore, the ^{15}N isotopic shift between $\delta^{15}N(NO_2)$ and $\delta^{15}N(NO_x)$ is given by:

$$\delta^{15}N(NO_2) - \delta^{15}N(NO_x) = \Delta^{15}(NO_2 - NO_x) = F_N \times (1 - f_{NO_2}) \quad (9)$$

Physico-chemical processes linking NO and NO_2 can preferentially either promotes or depletes ^{15}N in NO_2 with respect to emissions of NO_x (i.e. $\delta^{15}N(NO_2) \neq \delta^{15}N(NO_x)$). The importance of this fractionation shift is modulated by the factor ($1 - f_{NO_2}$). When NO is almost entirely converted into NO_2 ($f_{NO_2} \approx 1$), N fractionation effects can be neglected (i.e. $\delta^{15}N(NO_2) \approx \delta^{15}N(NO_x)$). From samples collected at Jülich, Germany, Freyer et al. (1993), observed for the first time the linear relation described by Eq. (8), and set the theoretical framework to interpret δ^{15}N variabilities in atmospheric NO_2. They showed that the observed seasonal variation of $\delta^{15}N(NO_2)$ was driven by N fractionation effects (represented in the F_N factor) caused by photochemistry and isotopic equilibrium. Based on this work, and that of Li et al. (2020), Albertin et al. (2021) derived an expression of F_N during the day assuming that the NO-NO_2 system is in isotopic equilibrium (steady-state):

$$(F_N)_{day} \approx \frac{\alpha_{LCIE}{}^{*} A^{*}{}_{day} + (\alpha_{EIE(NO_2/NO)} - 1)}{A^{*}{}_{day} + 1} \quad (10)$$

with $\alpha_{LCIE}{}^{*} = \alpha_{KIE(NO+O_3)} - \alpha_{PHIFE}$

and $A^{*}{}_{day} = \frac{J_{NO_2}}{k_{NO+NO_2}[NO]}$

where $\alpha_{LCIE}{}^{*}$ is the fractionation factor of combined KIE and PHIFE (LCIE is for Leighton Cycle Isotope Effect), and $\alpha_{EIE(NO_2/NO)}$ is the EIE fractionation factor between NO and NO_2. $\alpha_{EIE(NO_2/NO)}$ and $\alpha_{KIE(NO+O_3)}$ are temperature dependent and can be calculated following the theoretical approach of Walters and Michalski (2015) (Table D1). From calculations based on the zero point energy of $^{15}NO_2$ and the absorption cross section of $^{14}NO_2$, α_{PHIFE} is estimated to vary between 1.0020 and 1.0042 for a range of solar zenith angles between 90 and 0 ° (Fang et al. 2021). In this study we use a mean value

https://doi.org/10.5194/egusphere-2023-744
Preprint. Discussion started: 28 April 2023

of α_{PHIFE} at 1.0031. A^*_{day} is defined as the ratio of the NO_2 lifetime with respect to isotopic exchanges over the daytime NO_2 chemistry lifetime. J_{NO_2} is the NO_2 photolysis rate, k_{NO+O_3} is the rate constant of Reaction R3, and k_{NO+NO_2} is the rate constant of the isotopic exchange $^{15}NO_2 + {}^{14}NO \rightarrow {}^{14}NO_2 + {}^{15}NO$. During the day, $\Delta^{15}(NO_2 - NO_x)$ varies according to the environmental conditions. In low-NO_x conditions (e.g., remote and polar regions) $\Delta^{15}(NO_2 - NO_x)$ is predicted to be controlled by LCIE factors ($A^*_{\mathrm{day}} >> 1$), whereas an EIE-dominated regime ($A^*_{\mathrm{day}} << 1$) is expected in polluted environments (high-NO_x conditions).

At night, J_{NO_2} and α_{PHIFE} are null and A^*_{night} is defined as the ratio of the NO lifetime with respect to isotopic exchange with NO_2 over the nighttime NO chemical lifetime $\left(A^*_{\mathrm{night}} = \frac{k_{NO+O_3}[O_3]}{k_{NO+NO_2}[NO_2]}\right)$. In this study, we consider only one particular case with $A^*_{\mathrm{night}} << 1$, which means that isotopic exchanges are much faster than NO oxidation. In this scenario, KIE effects are negligible compared to EIE effects and $(F_N)_{\mathrm{night}}$ can be expressed as:

$$(F_N)_{\mathrm{night}} \approx \frac{(\alpha_{\mathrm{EIE}(NO_2/NO)} - 1)}{\alpha_{\mathrm{EIE}(NO_2/NO)}} \quad (11)$$

The complete derivation of Eq. (10) and Eq. (11) is given in Albertin et al. 2021.

Kinetic and equilibrium isotope effects are also expected during the conversion of NO_2 into NO_3^-. However, to date, no experimental study has reported on ^{15}N partitioning between atmospheric NO_2 and NO_3^-, and the enrichment factors are still being debated (Freyer 1991, Fang et al. 2021). Isotopic equilibrium is expected between N_2O_5 and NO_2 (Reaction R7) and the associated ^{15}N partitioning can be theoretically computed as a function of temperature (Walters and Michalski, 2015; Table D1). At 298 K, if N isotopic equilibrium is reached, N_2O_5 is predicted to have $\delta^{15}N$ values 27.6 ‰ higher than NO_2. Considering that the NO_2/NO_3^- isotopic fractionation through the N_2O_5 pathway is solely controlled by EIE, NO_3^- is therefore expected to be enriched in ^{15}N relative to NO_2.

Figure C1 schematises the dominant NO_x to NO_3^- conversion processes considered in this study, along with corresponding $\Delta^{17}O$ transfer factors and the known ^{15}N enrichment factors at 298 K (determined from both experimental and computational studies).

3 Results

3.1 General atmospheric observation

Surface temperatures during SP 1 and SP 2 show similar values, with a marked diurnal cycle (from −2 to 16 °C; Figure 1). A positive temperature gradient with altitude is observed from late evening to morning. Surface temperature rises around midday and reaches a maximum at around 15:00 LT, resulting in a negative temperature gradient with altitude. In deep

https://doi.org/10.5194/egusphere-2023-744
Preprint. Discussion started: 28 April 2023

Alpine valleys, the diurnal variability of surface air temperature is strongly influenced by the temporal evolution of the boundary layer structure, particularly in wintertime with the formation of a surface layer inversion (Whiteman, 1982). As previously observed in Chamonix (Chazette et al., 2005), the nocturnal surface layer inversion regularly thickens during the night of the sampling periods. After sunrise, air masses warm up until the nocturnal inversion layer breaks down in the late morning. Observed RH behaviour relatively correlates with the increase in temperature during the day, showing a rapid decrease between mid-morning and early afternoon (from 96 % to 23 % and from 96 % to 30 % for SP 1 and SP 2, respectively; Figure 1).

During SP 1 and SP 2, NO, NO_2 and O_3 mixing ratios (Figure 1) exhibit diurnal patterns typical for Chamonix in late February (Figure S3 in the Supplement) and of urban areas (Mayer, 1999). The highest NO level is observed in the morning, peaking at 10:30 LT (82 nmol mol^{-1} and 152 nmol mol^{-1} for SP 1 and SP 2, respectively). The concurrent increase in NO_2 and decrease in O_3 (down to 1 nmol mol^{-1}) can be attributed to Reaction R3 (NO + O_3). NO_x decrease in the late morning, likely due to a combination of lower emissions, NO_2 oxidation, and dilution effect. Meanwhile, O_3 gradually recovers to ca. 30 nmol mol^{-1}, a typical winter background air level in Europe (Gaudel et al., 2018). Due to local emissions, NO_x increase again from 16:00 LT, resulting in O_3 titration, and subsequently to an increase in NO_2 (up to 40 nmol mol^{-1}). After 18:30 LT, NO remains low until the morning, and NO_2 decreases slowly until midnight, stalls around 10 nmol mol−1, and then rises again at 5:30 LT. After the late afternoon titration, O_3 gently recovers at stay relatively low along the night likely due to a titration effect from nocturnal NO emissions which are confined in the surface layer inversion.

PM mass concentration patterns show differences between SP 1 and SP 2, with in average PM_{10} three times higher during SP 2 ((59.4 ± 37.6) µg m^{-3}) than during SP 1 ((20.6 ± 10.2) µg m^{-3}) (Figure 1). Both SP 1 and SP 2 show diurnal variations in PM, with morning and evening peaks related to local emissions from traffic and home heating (Aymoz et al., 2007). PM_{10} display an additional increase at midday following the breakdown of the temperature inversion. At 12:30 LT, while PM_{10} increase moderately during SP 1 to reached 38.6 µg m^{-3}, a large increase to 119 µg m^{-3} is observed during SP 2. Then PM_{10} decrease during the afternoon of SP 1, but remained elevated during the afternoon of SP 2 until the formation of the surface inversion layer. The considerable increase in PM_{10} between SP 1 and SP 2 suggests that the origin of the source is probably outside of the valley. It turns out that a Saharan dust episode began on February 23 (Fig. S3 in the Supplement). Saharan dust deposition is a well-known phenomenon in the Alps, which is characterised by a sudden increase of coarse particles, mainly composed of alumino-silicates as well as calcium and potassium (Angelisi and Gaudichet, 1991; Delmas, 1994; Di Mauro et al., 2019; Goudie and Middleton, 2001; Greilinger et al., 2018; Schwikowski et al., 1995; Sodemann et al., 2006).

The NO_3^- mass concentration varies from 0.3 µg m^{-3} to 3.4 µg m^{-3}, with an average of (0.9 ± 0.6) µg m^{-3} for SP 1 and of (1.2 ± 0.9) µg m^{-3} for SP 2 (Figure 1). During both sampling periods, NO_3^- is within the range of previous observations made in Chamonix in winter (Allard, 2018). NO_3^- shows a distinctive peak at 3.4 µg m^{-3} during SP 2 between 10:30 and 13:30 LT, correlated with the PM_{10} surge. During transportation, dust can undergo heterogeneous uptake and conversion of gases on its surface, leading to the inclusion of secondary species such as NO_3^-, sulfate, and ammonium (Usher et al., 2003). NO_3^- on

https://doi.org/10.5194/egusphere-2023-744
Preprint. Discussion started: 28 April 2023

dust results mainly from HNO_3 uptake and heterogeneous reactions of N_2O_5 (see Usher et al., 2003 for a review and references therein). Mineral dust is believed to significantly contribute to NO_3^- formation and size distribution, particularly in regions close to dust emission sources (Karydis et al., 2016). However, the origin of NO_3^- during SP 2 at our site remains unclear and could be attributed to the advection of both nitrated-dust particles formed through heterogeneous processes during transport and anthropogenic fine particles (Aymoz et al. 2004).

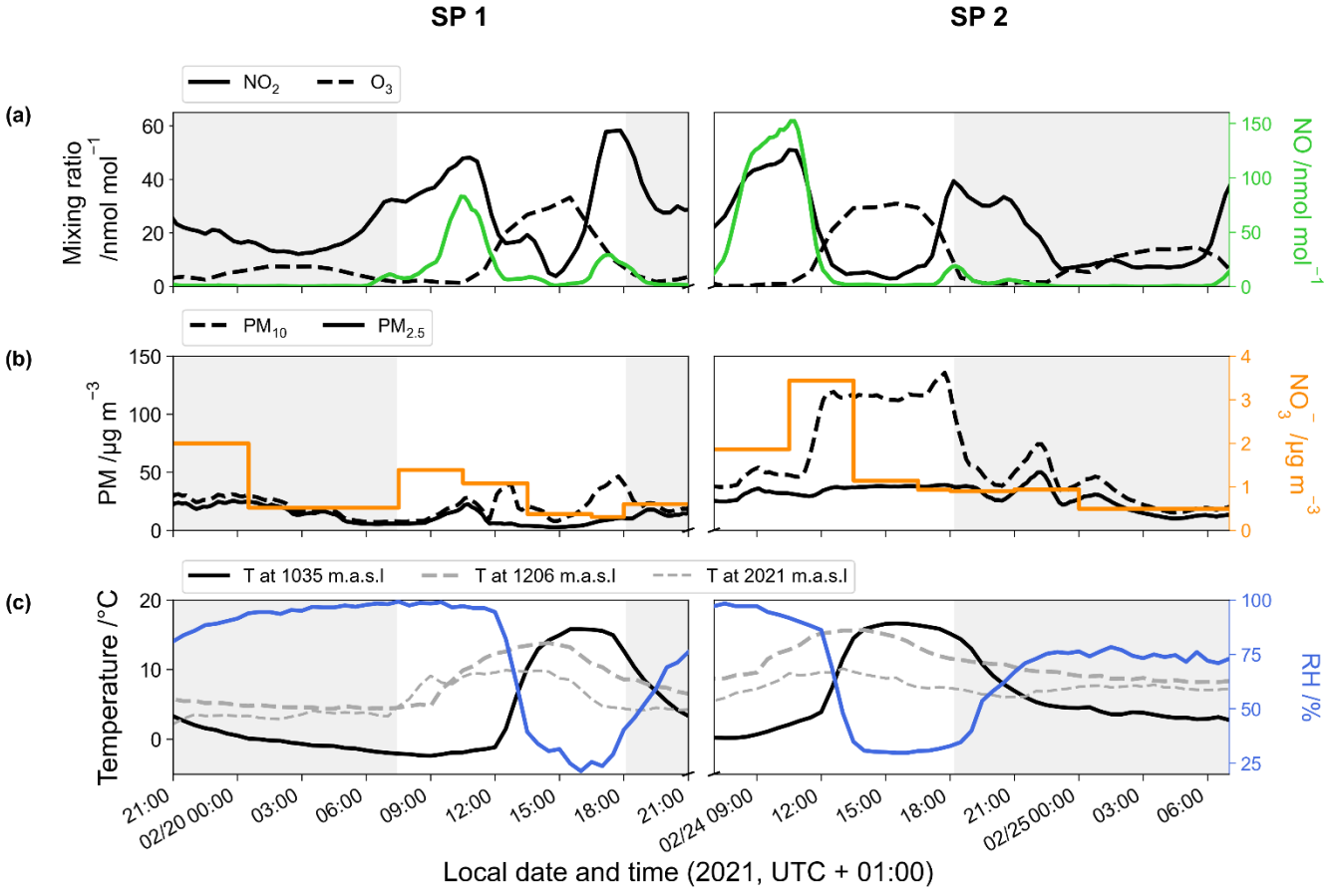

Figure 1. Temporal evolution of the 1-hour rolling mean of **(a)** NO_2 (black line), O_3 (dashed line) and, NO (green line) mixing ratio, **(b)** PM (dashed line for PfM_{10} and solid line for $PM_{2.5}$) and NO_3^- (orange horizontal line) mass concentration and **(c)** temperature at the surface (black line), at 1206 m.a.s.l (dashed grey line), and at 2021 m.a.s.l (light dashed grey line) and surface relative humidity (blue line). Data were collected during the two sampling periods (SP 1 and SP 2) in Chamonix. Grey backdrop shaded areas represent the nighttime.

3.2 Isotopic composition of atmospheric NO_2 and NO_3

Figure 2 shows the temporal evolution of measured $\Delta^{17}O$ and $\delta^{15}N$ of NO_2 and NO_3^- in Chamonix during the two sampling days (SP 1 and SP 2). All isotopic data used in this study are reported in Table S1 and Table S2 in the Supplement.

https://doi.org/10.5194/egusphere-2023-744
Preprint. Discussion started: 28 April 2023

3.2.1 Oxygen isotopic composition

Over the course of SP 1 and SP 2, $\Delta^{17}O(NO_2)$ shows a large diurnal variability (from 19.6 ‰ to 40.8 ‰) with a (weighted mean ± one standard deviation) of (25.2 ± 7.1) ‰. $\Delta^{17}O(NO_2)$ values during the day (7:30–18:00 LT, (28.5 ± 7.3) ‰) are significantly higher (p-value = 0.002, n = 16) than during the night (18:00–7:30 LT, (20.8 ± 1.0) ‰). $\Delta^{17}O(NO_2)$ values are similar during daytime SP 1 and SP 2, except for the 7:30–10:30 LT interval (29.4 ‰ and 22.3 ‰ for SP 1 and SP 2, respectively). For both sampling periods, after sunset, $\Delta^{17}O(NO_2)$ drop rapidly to stabilize between 21:00 and 7:30 LT at ca. 20 ‰. According to Eq. (5), the drop of $\Delta^{17}O(NO_2)$ in the early evening reflects the rapid turnover of NO_2 formed during the day by NO_2 produced during the night via the conversion of freshly emitted NO. High NO_2 throughout the night, along with relatively low O_3, supports observations of low $\Delta^{17}O(NO_2)$ at night (i.e. ≈20 ‰). Using the same method in a mid-latitude urban area in spring, Albertin et al. (2021) reported very similar $\Delta^{17}O(NO_2)$ values over the course of one day (20.5–39.2 ‰), following a comparable diurnal pattern.

$\Delta^{17}O(NO_3^-)$ varies significantly along a similar diurnal scheme (from 18.3 ‰ to 28.1 ‰), with a weighted mean of (22.5 ± 3.1) ‰. Nevertheless, unlike $\Delta^{17}O(NO_2)$, daytime and nighttime $\Delta^{17}O(NO_3^-)$ mean values are not significantly different (p-value > 0.05, n = 14). Furthermore, while $\Delta^{17}O(NO_2)$ values are relatively similar during the two sampling periods, $\Delta^{17}O(NO_3^-)$ values are systematically higher during SP 2 than during SP 1, except during the 7:30–10:00 LT interval. Observed $\Delta^{17}O(NO_3^-)$ values in Chamonix are in the same range as those previously measured in urban environments, but lower than most values measured during the cold season, which are typically >25 ‰ (see Savard et al. 2018 and references therein). From wintertime high-time-resolved (3 h) aerosol sampling in Beijing, Zhang et al. (2022) reported $\Delta^{17}O(NO_3^-)$ values between 23.4 ‰ to 39.3 ‰, with higher values observed at night ((31.0 ± 2.6) ‰) than during the day ((29.3 ± 3.0) ‰). This diel behaviour of $\Delta^{17}O(NO_3^-)$ values was attributed to the influence of nocturnal and photochemical reactions on NO_3^- formation. In Chamonix, the range of $\Delta^{17}O(NO_3^-)$ values are very different from Zhang et al. (2022) observations, with consistently lower values and a distinct diurnal tendency. However, in the cases of $\Delta^{17}O(NO_3^-)$ observations at sub-daily temporal scale, the atmospheric lifetime of NO_x and NO_3^- is critical for comparing $\Delta^{17}O(NO_3^-)$ observations from one site to another. Pollutant levels and atmospheric conditions between Chamonix and Beijing are very different. Notably in wintertime, Asian urban areas can experience severe haze pollution events with NO_3^- mass concentration exceeding 70 μg m^{-3}, which is over 10 times higher than in Chamonix (Zhang et al., 2022b; Lim et al., 2022; He et al., 2018). During such events, PM can reach several hundreds of μg m^{-3} for several days, which can significantly impact the atmospheric processes involved in the formation of species, and their lifetime in the atmospheric boundary layer. Aside the intrusion of Saharan dust during SP 2, the pollutant level in Chamonix is indicative of a moderately polluted region, with significant diurnal variation.

https://doi.org/10.5194/egusphere-2023-744
Preprint. Discussion started: 28 April 2023

3.2.2 Nitrogen isotopic composition

Over the two sampling periods, $\delta^{15}N(NO_2)$ shows substantial diurnal variability (from −10.0 to 19.7 ‰) with a weighted mean of (4.0 ± 9.1) ‰. Albertin et al. (2021) reported a weak diurnal cycle of $\delta^{15}N(NO_2)$, in a narrow range from about −12 to −10 ‰. Similarly, Walters et al. (2018) observed in a urban/suburban location in summer an overall mean $\delta^{15}N(NO_2)$ value of (−11.4 ± 6.9) ‰. From Eq. (8), $\delta^{15}N(NO_2)$ should reflect the variability of NO_x emission sources and/or N fractionation effects between emitted NO_x and NO_2 weighted by the ratio f_{NO_2} (see Section 2.4). In the two previous works, isotope effects were small (<2.7 ‰). Interestingly, at our site f_{NO_2} shows a wider range, from 0.3 to 1, with minimum and maximum value correlating with the highest and lowest $\delta^{15}N(NO_2)$, respectively, suggesting significant N isotopic fractionation effects (Freyer et al., 1993).

$\delta^{15}N(NO_3^-)$ also exhibits substantial variability during the day, ranging from −1.3 to 14.9 ‰ and from −4.2 to 9.2 ‰ during SP 1 and SP 2, respectively. At night, $\delta^{15}N(NO_3^-)$ values show less variability, with an overall mean of (1.4 ± 1.2) ‰ and (−1.1 ± 0.4) ‰ during SP 1 and SP 2, respectively. $\delta^{15}N(NO_3^-)$ are within the range of observations reported in urban areas (He et al., 2020; Zhang et al., 2022a). A similar diurnal pattern was observed in samples collected during a cruise along the Californian coast in spring 2010 (Vicars et al., 2013), and isotopic exchanges between NO and NO_2 during the day were targeted to be the primary driver of the diel variability.

The temporal evolution of $\Delta^{17}O(NO_2)$ and $\Delta^{17}O(NO_3^-)$ are interpreted in section 4.1 and 4.2, respectively. In section 4.3, N fractionation effects between emitted NO_x and NO_2 are quantified, and the nature of the dominant NO_x emission source is estimated. Finally, in section 4.4 is described the dynamics of $\delta^{15}N(NO_3^-)$. The use of $\delta^{15}N(NO_3^-)$ to trace NO_x emission sources and oxidation processes is also discussed.

https://doi.org/10.5194/egusphere-2023-744
Preprint. Discussion started: 28 April 2023

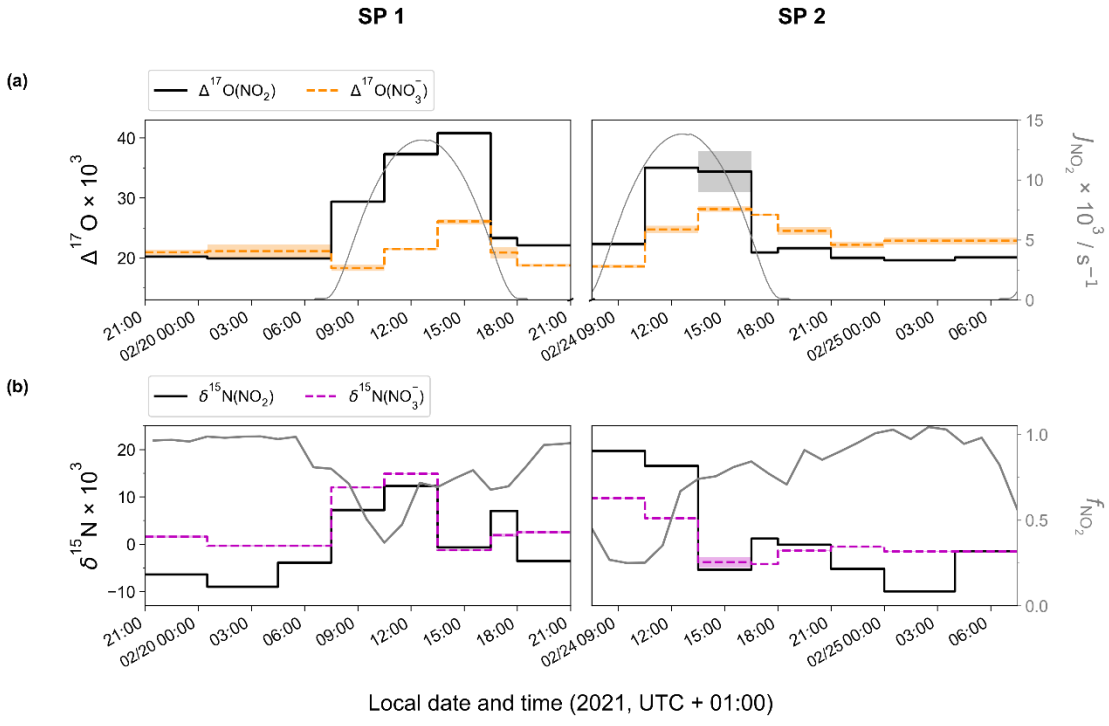

Figure 2. Temporal evolution of **(a)** $\Delta^{17}O$ and **(b)** $\delta^{15}N$ of atmospheric NO_2 (top and bottom solid black horizontal line) and NO_3^- (top orange and bottom magenta horizontal dashed line) in Chamonix. (length of horizontal line = sampling period, shaded area = overall analytical error). The NO_2 photolysis rate (J_{NO_2}, top grey line) is from CiTTyCAT boxmodel output. f_{NO_2} (f_{NO_2} = [NO_2] / ([NO_2] + [NO]); bottom grey line) is calculated from hourly mean mixing ratio of NO and NO_2.

4 Discussion

4.1 $\Delta^{17}O$ and diurnal cycling of atmospheric NO_2

Using Eq. (3), we can derive from daytime $\Delta^{17}O(NO_2)$ the relative contribution of Reaction R3 (NO + O_3) and Reaction R4 (NO + RO_2) to the formation of NO_2 (T_{NO+O_3}):

$$T_{NO+O_3} = \frac{\Delta^{17}O_{day}(NO_2)}{\Delta^{17}O_{NO+O_3}(NO_2)} \quad (12)$$

Combining Eq. (3) and Eq. (4) we can further derive the corresponding RO_2 mixing ratio following:

$$[RO_2] = \frac{k_{NO+O_3}[O_3]}{k_{NO+RO_2}}\left(\frac{\Delta^{17}O_{NO+O_3}(NO_2)}{\Delta^{17}O_{day}(NO_2)} - 1\right) \quad (13)$$

https://doi.org/10.5194/egusphere-2023-744
Preprint. Discussion started: 28 April 2023

The choice of the $\Delta^{17}O_{NO+O_3}(NO_2)$ is of a particular importance for quantifying T_{NO+O_3}, and therefore for RO_2. In the literature, the value derived for $\Delta^{17}O_{NO+O_3}(NO_2)$ varies between 35 and 41 ‰ (Michalski et al., 2003; Savarino et al., 2016; Vicars et al., 2012; Zhang et al., 2022b; Li et al., 2022a). On the basis of their maximum daytime observation of $\Delta^{17}O(NO_2)$, Albertin et al. (2021) used a $\Delta^{17}O_{NO+O_3}(NO_2)$ value of 39.2 ‰ assuming that this value reflects the conversion of NO to NO_2 only through Reaction R3 (NO + O_3). Given ours respective analytical uncertainties (around ±1 ‰), this value is in very good agreement with the maximum daytime value of 40.8 ‰ observed in Chamonix. Therefore, we assume that the highest daytime $\Delta^{17}O(NO_2)$ value at our site corresponds to $T_{NO+O_3} \approx 1$ leading to $\Delta^{17}O_{NO+O_3}(NO_2)$ = 40.8 ‰. Using the experimental $\Delta^{17}O_{NO+O_3}(NO_2)$ transfer function determined by Savarino et al. (2008) ($\Delta^{17}O_{NO+O_3}(NO_2)$= 1.18 ± 0.07 × $\Delta^{17}O(O_3)_{bulk}$ + (6.6 ± 1.5) ‰) we estimate the bulk O_3 isotopic anomaly ($\Delta^{17}O(O_3)_{bulk}$) at (29.0 ± 2.2) ‰. This value is consistent with previously reported values in the literature (Vicars and Savarino, 2014; Krankowsky et al., 1995; Johnston and Thiemens, 1997).

Between 7:30 and 16:30 LT, T_{NO+O_3} varies from 0.55 to 1.00 (Table 1). The NO + O_3 pathway is dominant between 10:30 and 16:30 LT, when O_3 is highest (Figure 1), while the maximum contribution for the NO + RO_2 pathway is observed between 7:30 and 10:30 LT. Between 7:30 and 16:30 LT, we estimate an average RO_2 mixing ratio at our site of (0.88 ± 0.88) pmol mol^{-1} and (4.92 ± 5.16) pmol mol^{-1} during SP 1 and SP 2, respectively. Studies conducted in urban winter environments measured RO_2 mixing ratios at a few pmol mol^{-1}, in good agreement with our estimations (Ren et al., 2006; Emmerson et al., 2005; Tan et al., 2018; Kanaya et al., 2007). To further assess the representativeness of our RO_2 estimates from $\Delta^{17}O(NO_2)$ observations (Case A), we also calculate RO_2 from the empirical formula of Kanaya et al., 2007 (Case B):

$$[HO_2] \,/\, \text{pmol mol}^{-1} = e^{(5.7747\times10^{-2} \times [O_3]\,/\text{nmol mol}^{-1} - 1.7227)} \quad (14)$$

using a $[RO_2]/[HO_2]$ ratio of 0.859 (Zhang et al., 2022b), and the O_3 mixing ratio average over each NO_2 sampling periods. Furthermore, we compare the T_{NO+O_3} values calculated from Eq. (12) (Case A) and from Eq. (4) (using RO_2 calculated empirically; Case B). These results are reported in Table 1. Between 7:30 and 16:30 LT, RO_2 is relatively consistent between Case A and Case B. To note, comparison of the absolute value between Case A and Case B show substantial discrepancies, particularly for the sample collected on Feb 24 between 13:30 and 16:30, which could be due to the important blank associated with this sample. However, the overall mean value between 7:30 and 16:30 LT lay in the ranged of uncertainty. The calculated T_{NO+O_3} values show a consistent pattern for both methods, with the lowest values observed between 7:30–10:30 LT.

The highest contribution of RO_2 in the oxidation of NO into NO_2 is correlated with the highest NO levels. Interestingly, previous studies reported a high sensitivity of RO_2 to changes in NO_x, particularly at high NO_x levels (Ren et al., 2006; Stone et al., 2012). The source of RO_2 in wintertime is mainly driven by the production of OH radicals from HONO photolysis,

https://doi.org/10.5194/egusphere-2023-744
Preprint. Discussion started: 28 April 2023

alkene ozonolysis, and formaldehyde photolysis (Tan et al., 2018). During wintertime, HONO plays a crucial role in $NO_x/O_3/RO_2$ chemistry, particularly in the morning, as its photolysis can potentially accelerate daytime oxidation processes, as for VOCs, leading to increased RO_2 production (Alicke et al., 2003; Aumont et al., 2003). Direct emissions from vehicle exhaust could be significant a source of VOCs and HONO at our site (Brulfert et al., 2005; Gu et al., 2019; Kirchstetter et al., 1996; Kurtenbach et al., 2001; Liu et al., 2023). Heterogeneous processes on ground surfaces and aerosols can also contribute to HONO formation (Aumont et al., 2003). In addition, snowpack releases may also be a potential source of HONO (Grannas et al., 2007), as detected in Paris after a snow event, which could significantly impact the urban OH budget (Michoud et al. 2015).

Overall, the closeness between RO_2 estimates using $\Delta^{17}O(NO_2)$ observations and those from empirical calculations and other site observations, confirm the sensitivity of $\Delta^{17}O(NO_2)$ to $NO_x/O_3/RO_2$ chemical dynamics. We believe that this method can be use to a better understanding of the oxidation processes of N_r species, down to a sub-daily temporal scale.

Sampling interval (start - end)	T_{NO+O_3}		RO_2 /pmol mol^{-1}	
	Case A[(1)]	Case B[(2)]	Case A[(1)]	Case B[(2)]
20/02 07:30 - 20/02 10:30	0.72 ± 0.01	0.86 ± 0.11	0.86 ± 0.75	0.37 ± 0.03
20/02 10:30 - 20/02 13:30	0.91 ± 0.01	0.96± 0.01	1.77 ± 0.36	0.74 ± 0.06
20/02 13:30 - 20/02 16:30	1.00 ± 0.01	0.97 ± 0.01	0.00 ± 0.91	1.79 ± 0.15
Mean	*0.88*	*0.97*	*0.88*	*0.97*
Std dev.	*0.14*	*0.73*	*0.88*	*0.73*
24/02 07:30 - 24/02 10:30	0.55 ± 0.01	0.67 ± 0.70	0.58 ± 1.67	0.35 ± 0.03
24/02 10:30 - 24/02 13:30	0.86 ± 0.01	0.97 ± 0.01	3.56 ± 0.50	0.76 ± 0.07
24/02 13:30 - 24/02 16:30	0.84 ± 0.08	0.97 ± 0.11	10.63 ± 6.75	1.90 ± 0.16
Mean	*0.75*	*1.00*	*4.92*	*1.00*
Std dev.	*0.18*	*0.81*	*5.16*	*0.81*

(1) RO_2 is estimated from Eq. (13) using $\Delta^{17}O(NO_2)$, $\Delta^{17}O_{NO+O_3}(NO_2)$ = 40.8 ‰ and O_3 measurements. T_{NO+O_3} is derived from Eq. (12) and $\Delta^{17}O(NO_2)$ measurements.
(2) RO_2 is estimated from Eq. (14), using measured O_3 mixing ratio and a $[RO_2]/[HO_2]$ ratio of 0.859. T_{NO+O_3} is derived from Eq. (3) using calculated RO_2 from the empirical formula.

Table 1. Comparison of calculated RO_2 mixing ratio and T_{NO+O_3} (mean value ± overall uncertainty) using the isotopic and the empirical theoretical approach.

https://doi.org/10.5194/egusphere-2023-744
Preprint. Discussion started: 28 April 2023

4.2 Interpretation of $\Delta^{17}O(NO_3^-)$ diurnal variations

4.2.1 Daytime and nighttime steady state evaluation of $\Delta^{17}O(NO_3^-)$

To investigate the factors influencing the variability of $\Delta^{17}O(NO_3^-)$ at our site, one can compare observations of $\Delta^{17}O(NO_3^-)$ with an estimation of $\Delta^{17}O(NO_3^-)$ derived from $\Delta^{17}O$ mass balance equations constrained by observations of $\Delta^{17}O(NO_2)$, and representative of the main daytime and nighttime chemistry processes.

During the day, we consider that the conversion of NO_2 into NO_3^- is predominantly influenced by Reaction R5 (OH pathway), and the theoretical corresponding ^{17}O-excess transfer to NO_3^- is estimated using Eq. (6). Then, in order to estimate a mean daytime $\Delta^{17}O(NO_3^-)$ representative of the potential to produce NO_3^- from surface NO_2 through the OH pathway between 7:30 and 16:30 LT, each calculated $\Delta^{17}O(NO_3^-)$ value (n = 3 per sampling day) is weighted by the product $[NO_2]\times J_{NO_2}$, assuming that the diurnal variability of the OH mixing ratio follows the J_{NO_2} diurnal variation (Liu et al., 2021). Finally, the overall mean daytime $\Delta^{17}O(NO_3^-)$ value for SP 1 and SP 2 is estimated by taking the sum of the weighted calculated values ($=\Delta^{17}O_{calc}(NO_3^-)$). The same approach is used during the night assuming that the conversion of NO_2 into NO_3^- is dominated by Reactions R6–R8 (N_2O_5 pathway). Eq. (7) is used to estimate the corresponding $\Delta^{17}O(NO_3^-)$ and each calculated $\Delta^{17}O(NO_3^-)$ value between 21:00 and 4:30 LT (n = 2 per sampling day) is weighted by the product $[NO_2]\times[O_3]$. The ^{17}O-excess transferred from O_3 to NO_2 during Reaction R6 ($\Delta^{17}O_{NO_2+O_3}(NO_3)$) is fixed at 44.7 ‰. This value is set accordingly to the transfer function reported by Berhanu et al. (2012) whereby $\Delta^{17}O_{NO_2+O_3}(NO_2)$ = (1.23 ± 0.19) × $\Delta^{17}O(O_3)_{bulk}$ + (9.02 ± 0.99) and $\Delta^{17}O(O_3)_{bulk}$ = 29.0 ‰. As $\Delta^{17}O_{calc}(NO_3^-)$ values are derived from $\Delta^{17}O(NO_2)$ observations, in order to be as representative as possible with respect to the conversion time of NO_2 to NO_3^- through the OH and N_2O_5 pathways, we compare hereafter $\Delta^{17}O_{calc}(NO_3^-)$ values with observed $\Delta^{17}O(NO_3^-)$ starting 3 hours later. Hence, during the day, $\Delta^{17}O_{calc}(NO_3^-)$ is compared with $\Delta^{17}O(NO_3^-)$ observations averaged between 10:30 and 18:30 LT (n = 2). At night, $\Delta^{17}O_{calc}(NO_3^-)$ is compared with the single $\Delta^{17}O(NO_3^-)$ observation covering the period from midnight to 7:30 LT.

At night during SP 1, $\Delta^{17}O(NO_3^-)$ and $\Delta^{17}O_{calc}(NO_3^-)$ are in very good agreement ($\Delta^{17}O_{calc}(NO_3^-) - \Delta^{17}O(NO_3^-) = \Delta^{17}(NO_3^-_{calc} - NO_3^-_{obs}) = -0.7$ ‰), suggesting a local and rapid (< 12 h) conversion of NO_2 into NO_3^- via the N_2O_5 pathway. During the day, observed $\Delta^{17}O(NO_3^-)$ is 1.2 ‰ lower than $\Delta^{17}O_{calc}(NO_3^-)$. This small difference between observed and calculated $\Delta^{17}O$ of NO_3^- during the day could be explained by the presence of NO_3^- residues formed during the previous night, which are not considered in the calculations since they do not account for NO_3^- lifetime. An additional input of NO_3^- formed aloft during the previous night is also plausible and is discussed in the next section.

In contrast to SP 1, $\Delta^{17}O_{calc}(NO_3^-)$ values during SP 2 are significantly lower than observations, particularly during the day with a $\Delta^{17}(NO_3^-_{calc} - NO_3^-_{obs})$ of –6.3 ‰. To note, ambient NO_2 is low for the NO_2 sample collected on Feb 24 between 13:30 and 16:30, therefore, the incertitude related its blank has little influence on the daily average of $\Delta^{17}O_{calc}(NO_3^-)$ as it is pondered by the mean ambient NO_2 mixing ratio of each sampling interval. Since the daytime NO_2 to

https://doi.org/10.5194/egusphere-2023-744
Preprint. Discussion started: 28 April 2023

NO_3^- oxidation process is not expected to be drastically different between SP 1 and SP 2, the difference of behaviour between SP 1 and SP 2 suggest different origins of NO_3^-. Although less important than during the day, at night, $\Delta^{17}O_{calc}(NO_3^-)$ values for SP 2 is lower by 2.4 ‰ to the observed value. Similarly, as nighttime NO_2 to NO_3^- oxidation processes are not expected to be different between SP 1 and SP 2, this small shift can be explained by residuals of daytime NO_3^-.

According to these results, during SP 1, observed $\Delta^{17}O$ of NO_3^- can be explained by the local and rapid (< 12 h) oxidation of NO_2, dominated by the OH and N_2O_5 pathway during the day and the night, respectively. However, in contrast to SP 1, the ^{17}O-excess measured in NO_3^- during the day of SP 2 cannot be fully constrained by the oxidation of surface NO_2 through the OH pathway, suggesting the presence of NO_3^- not formed at the surface.

	Day		*Night*	
	SP 1	SP 2	SP 1	SP 2
$\Delta^{17}O(NO_2)^{(1)}$ /‰	34.2 ± 5.0	27.4 ± 6.7	19.9 ± 0.0	29.8 ± 0.3
$\Delta^{17}O(NO_3^-)^{(2)}$ /‰	22.4 ± 2.3	25.8 ± 1.7	21.1	22.8
$\Delta^{17}O_{calc}(NO_3^-)^{(3)}$ /‰	23.6 ± 3.2	19.5 ± 4.0	20.7 ± 0.0	20.7 ± 0.2
$\Delta^{17}(NO_{3\,calc}^- - NO_{3\,obs}^-)$ /‰	1.2	–6.3	–0.7	–2.4

(1) Mean observed $\Delta^{17}O(NO_2)$ between 7:30–16:30 LT at day and between 21:30–4:30 LT at night
(2) Mean observed $\Delta^{17}O(NO_3^-)$ between 10:30–18:00 LT at day and between 00:00–7:30 LT at night
(3) Mean calculated $\Delta^{17}O(NO_3^-)$ using Eq. (6) at day and Eq. (7) at night, and observed $\Delta^{17}O(NO_2)$. Day and night calculated values were pondered by $[NO_2]\times J_{NO_2}$ and by $[NO_2]\times[O_3]$, respectively

Table 2. Mean observed $\Delta^{17}O$ data of NO_2 ($\Delta^{17}O(NO_2)$) and NO_3^- ($\Delta^{17}O(NO_3^-)$) in Chamonix, and mean calculated $\Delta^{17}O$ of NO_3^- ($\Delta^{17}O_{calc}(NO_3^-)$)

1.1.1 $\Delta^{17}O(NO_3^-)$ sub-daily dynamics

$\Delta^{17}O(NO_3^-)$ values for the 7:30–10:30 LT interval are very similar between SP 1 (18.3 ‰) and SP 2 (18.5 ‰), unlike the 10:30–12:30 LT interval during which $\Delta^{17}O(NO_3^-)$ values are significantly different (21.4 ‰ and 24.7 ‰ for SP1 and SP2, respectively). The more pronounced enhancement of $\Delta^{17}O(NO_3^-)$ during the 10:30–12:30 LT interval of SP 2 suggests the presence of NO_3^- not formed from the oxidation of local NO_2 at the surface, as mentioned previously. One more piece of evidence is that during this period of time, PM_{10} and NO_3^- levels increase significantly alongside the disruption of the inversion layer (depicted in Fig. 3.1). It can be inferred that this rise in PM_{10} is mostly due to the presence of Saharan dust. The simultaneous increase of NO_3^- and of $\Delta^{17}O(NO_3^-)$ corroborate the hypothesis that this NO_3^- was not formed locally. Furthermore, such an increase in $\Delta^{17}O(NO_3^-)$ by surface processes can only be supported by the oxidation of surface NO_2

https://doi.org/10.5194/egusphere-2023-744
Preprint. Discussion started: 28 April 2023

through the N_2O_5 pathway, which is not expected to be important at this period of time due to the rapid photolysis of NO_3 and its titration by NO (Brown and Stutz, 2012).

Interestingly, aerosol samplings conducted at various heights (8, 120, and 260 m.a.g.l) in Beijing, China, showed a positive vertical gradient in $\Delta^{17}O$ values of NO_3^- in winter, from in average 29 to 33 ‰ (Fan et al., 2022), while summertime values more homogeneous. In summer time, the values at the three levels are very close This increase of $\Delta^{17}O(NO_3^-)$ with attitude is believed to result from a stratification of NO_2 to NO_3^- oxidation processes due to low vertical mixing during winter with elevated surface NO_x emissions. However, the authors did not account for the potential variability of $\Delta^{17}O(NO_2)$ values, which can be substantial on a vertical scale due to the expected low surface $\Delta^{17}O(NO_2)$ values in urban areas at night. For this study, we propose an alternative interpretation of the vertical dynamics of $\Delta^{17}O(NO_3^-)$ values, where $\Delta^{17}O(NO_2)$ is considered as the main driver. During the formation of the nocturnal boundary layer, NO_2 formed during the day can be trapped above the surface layer in the nocturnal residual layer (NRL). This NO_2 has a high $\Delta^{17}O$ because it was formed during the previous days at PSS. Throughout the night, this highly enriched NO_2 (ca. 37 ‰ which is the average of the maximum values of SP 1 and SP 2) is converted to NO_3^- via the N_2O_5 pathway, leading to a substantial $\Delta^{17}O$ transfer to NO_3^- at around 32 ‰, which is in the range of Fan et al. (2022) values. In the meantime, nighttime surface emissions of NO_x are converted into NO_2 by O_3 with a $\Delta^{17}O$ transfer of ca. 20 ‰. This low enriched NO_2 is further converted to NO_3^- by the N_2O_5 pathway, resulting in a $\Delta^{17}O$ transfer at around 21 ‰. NO_2 with low $\Delta^{17}O$ value (≈ 20 ‰) is very likely to be formed only at the surface during the night in areas experiencing important nighttime NO_x emissions (Michalski et al., 2014). Furthermore, surface NO_2 with low $\Delta^{17}O$ is not expected to be transported aloft as it is formed during the night in the surface inversion layer. Therefore, NO_3^- formed in the NRL during winter nights may be more enriched than the NO_3^- formed concurrently at the surface, regardless of the NO_2 oxidation processes involved. When the inversion layer breaks during the following day, the NO_3^- that was formed in the NRL during the night is mixed with the NO_3^- formed at the surface, resulting in an increase in the overall surface $\Delta^{17}O$. In this scenario, the presence of the Saharan dust during SP 2 may have increased the deposition of NO_3^- formed aloft, in comparison to SP 1. Such $\Delta^{17}O$ dynamics at night could explain the observed increase in $\Delta^{17}O$ of NO_3^- at the surface following the collapse of the nocturnal inversion layer. However, we cannot determine whether the enriched NO_3^- were formed in the vicinity of Chamonix and/or transported to our site by Saharan dust.

Although the exact nature of the high ^{17}O anomalies measured in NO_3^- during SP 2 remains unclear, boundary layer dynamics is thought to play a significant role in the variability of $\Delta^{17}O(NO_3^-)$ due to the stratification of NO_2. Therefore, a wider consideration of such factors should be considered to avoid possible over-interpretation of $\Delta^{17}O(NO_3^-)$ variabilities, especially in urban areas in winter experiencing significant boundary layer dynamics and high nocturnal surface emissions of NO_x. Measuring $\Delta^{17}O(NO_2)$ at various altitudes could provide better insights on the vertical dynamics of $\Delta^{17}O(NO_3^-)$, and subsequently quantitative informations on NO_3^- production processes.

https://doi.org/10.5194/egusphere-2023-744
Preprint. Discussion started: 28 April 2023

4.3 δ^{15}N in atmospheric NO_2

Figure 3 shows the linear dependence of $\delta^{15}N(NO_2)$ on $(1 - f_{NO_2})$ over the two sampling periods, indicating the significant influence of atmospheric processes that alter the N isotopic distribution during the conversion of NO_x into NO_2. The linear regression gives a slope of about (43.7 ± 3.4) ‰ and an intercept of about (8.8 ± 1) ‰. According to Eq. (10) and Eq. (11), the linearity between daytime (07:30−18:00 LT) and nighttime (18:00−07:30 LT) values suggests that EIE dominates the N fractionation processes between NO_x and NO_2. However, there is more variability around the linear fit in the daytime observations than in the nighttime observations, which may be attributed to the influence of LCIE during the day.

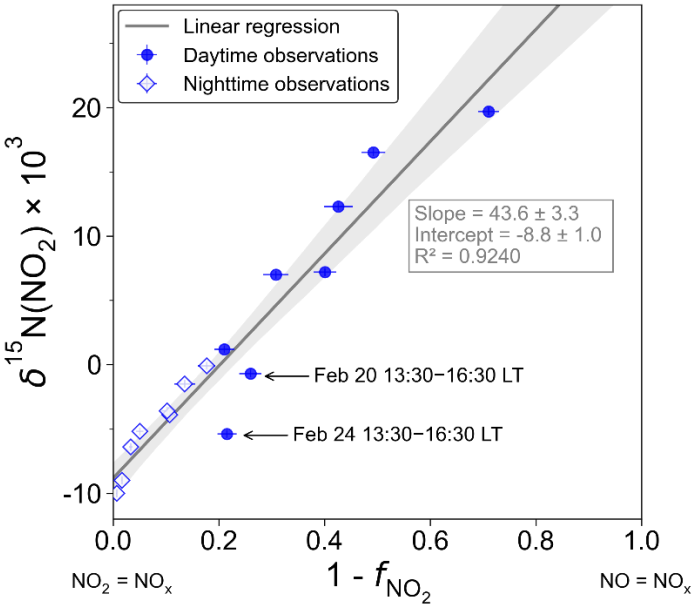

Figure 3. Correlation plot of δ^{15}N of atmospheric NO_2 vs. $(1 - f_{NO_2})$ from observations in Chamonix in February 2021. f_{NO_2} are averaged over the collection period of each NO_2 sample. The grey shade is the 95 % confidence interval. Diamonds and dots represent the nighttime (18:00−07:30 LT) and daytime (07:30−18:00 LT) observations, respectively. The linear regression line is plotted over the nighttime and daytime observations.

The relative importance of EIE and LCIE in the N fractionation between emitted NO_x and NO_2 is evaluated by calculating the daytime and nighttime A^* factor associated to each NO_2 samplings (Table 3). Overall, the A^* values are small (mean ± one standard deviation: 0.21 ± 0.51) and reflect an EIE-dominated regime characterized by high NO_x (Li et al., 2020). It is interesting to note that the highest A^* values are observed between 13:30 and 16:30 LT, and correspond to the two data points in Figure 3 that lie outside the 95 % confidence interval of the regression line. These findings suggest that EIE is the dominant N fractionation processes between NO_x and NO_2 during both day and night ($A^* < 0.46$), with the exception of mid-afternoon when LCIE competes with EIE ($A^* > 0.46$).

https://doi.org/10.5194/egusphere-2023-744
Preprint. Discussion started: 28 April 2023

To quantify the drivers of the overall N fractionation effect (F_N) between NO_x and NO_2, we dissociate the two samples collected between 13:30 and 16:30 LT into a different group (Group #1 = GP 1) from the other samples (Group #2 = GP 2). The F_N values for GP 1 and GP 2 are calculated using Eq. (10) (which combines LCIE and EIE regimes) and Eq. (11) (which considers only the EIE regime), respectively (data used for calculations can be found in Section 2.4.2 and in the Supplement). The F_N values for GP 1 and GP 2 are significantly different, with a mean of 16.39 ‰ and 42.31 ‰, respectively. The close match between the mean F_N value of GP 2 and the observed value ((43.6 ± 3.3) ‰; slope of the regression line in Fig. 3.3) provides strong evidence for the reliability of Eq. (3.12), as well as the $\alpha_{EIE(NO_2/NO)}$ expression used therein, in accurately describing the variation of $\delta^{15}N(NO_2)$ at our site. This result holds significant importance in confirming the theoretical N isotopic fractionation framework used in prior research studies.

From A^* values, a greater influence of LCIE in mid-afternoon could have contributed to the outlying of the two samples collected between 13:30 and 16:30 LT (GP 1). However, as mentioned above, the sample collected on Feb 24 between 13:30 and 16:30 LT had a significant blank therefore it cannot be confirmed with certainty that the reason this sample falls outside the 95 % confidence interval of the regression line is solely due to LCIE. Nevertheless, the overall conclusion that EIE dominates the variability of $\delta^{15}N(NO_2)$ at our site is not affected by this uncertainty.

The $\delta^{15}N$ shift in NO_2 relative to emitted NO_x ($\Delta^{15}(NO_2 - NO_x)$) is calculated for each individual sample. The mean atmospheric $\delta^{15}N$ of NO_x ($\delta^{15}N(NO_x)$) is then estimated by subtracting the $\Delta^{15}(NO_2 - NO_x)$ value from the observed $\delta^{15}N(NO_2)$ value. $\Delta^{15}(NO_2 - NO_x)$ varies greatly over the two sampling periods (from 0.7 to 30.7 ‰) with a mean value of ca. 9 ‰. $\delta^{15}N(NO_x)$ show much less variability with an overall mean at (−7.8 ± 1.9) ‰, in very good agreement with the value derived from the regression relationship (−8.8 ‰; intercept of the regression line in Figure 3). Therefore, there appears to be little variation in NO_x emission sources at our site, and the wide variability in $\delta^{15}N(NO_2)$ is mainly driven by important equilibrium post-emission isotopic effects.

https://doi.org/10.5194/egusphere-2023-744
Preprint. Discussion started: 28 April 2023

Sampling interval (start – end)	$A^{*(1)}$	$F_N^{(2)}$	f_{NO_2}	$\Delta(NO_2 - NO_x)^{(3)}$ /‰	$\delta^{15}N(NO_x)$ /‰
GP #1					
20/02 13:30 – 20/02 16:30	0.46 ± 0.08	25.00 ± 2.27	0.74 ± 0.02	6.5 ± 0.9	−7.2 ± 0.9
24/02 13:30 – 24/02 16:30	2.09 ± 0.39	6.90 ± 1.97	0.78 ± 0.02	1.5 ± 0.4	−6.9 ± 0.6
Mean	1.27	16.39	0.76	4.09	−7.1
Std dev	1.14	12.58	0.03	3.50	0.2
GP #2					
19/02 21:00 – 20/02 00:30	0.03 ± 0.01	43.06 ± 0.17	0.97 ± 0.01	1.4 ± 0.1	−7.8 ± 0.3
20/02 00:30 – 20/02 04:30	0.07 ± 0.01	43.51 ± 0.18	0.98 ± 0.01	0.7 ± 0.1	−9.7 ± 0.3
20/02 04:30 – 20/02 07:30	0.02 ± 0.01	43.78 ± 0.22	0.89 ± 0.01	4.7 ± 0.4	−8.6 ± 0.5
20/02 07:30 – 20/02 10:30	0.05 ± 0.01	43.92 ± 0.18	0.60 ± 0.02	17.6 ± 1.0	−10.4 ± 1.1
20/02 10:30 – 20/02 13:30	0.10 ± 0.02	43.06 ± 0.18	0.57 ± 0.02	18.4 ± 1.0	−6.1 ± 1.0
20/02 16:30 – 20/02 18:00	0.03 ± 0.01	39.97 ± 0.18	0.69 ± 0.02	12.3 ± 0.8	−5.3 ± 0.8
20/02 18:00 – 20/02 21:00	0.01 ± 0.01	41.75 ± 0.19	0.90 ± 0.01	4.3 ± 0.5	−7.9 ± 0.6
24/02 07:30 – 24/02 10:30	0.01 ± 0.01	43.21 ± 0.18	0.29 ± 0.02	30.7 ± 0.9	−11.9 ± 0.9
24/02 10:30 – 24/02 13:30	0.07 ± 0.01	41.95 ± 0.18	0.51 ± 0.02	20.6 ± 1.0	−4.1 ± 1.1
24/02 16:30 – 24/02 18:00	0.16 ± 0.03	39.80 ± 0.16	0.79 ± 0.02	8.4 ± 0.6	−7.2 ± 0.7
24/02 18:00 – 24/02 21:00	0.01 ± 0.01	40.88 ± 0.18	0.82 ± 0.02	7.2 ± 0.6	−7.3 ± 0.6
24/02 21:00 – 25/02 00:00	0.03 ± 0.02	42.20 ± 0.19	0.95 ± 0.01	2.1 ± 0.3	−7.3 ± 0.4
25/02 00:00 – 25/02 04:00	0.19 ± 0.03	42.48 ± 0.18	0.99 ± 0.01	0.3 ± 0.1	−10.3 ± 0.3
25/02 04:00 – 25/02 07:30	0.09 ± 0.01	42.69 ± 0.17	0.86 ± 0.02	5.8 ± 1.0	−7.3 ± 1.0
Mean	0.06	42.31	0.77	9.6	−7.9
Std dev	0.06	1.32	0.21	9.1	2.0

(1) Calculated from A^*_{day} between 7:30–18:00 LT and from A^*_{night} between 18:00–07:30 LT (A^*_{day} and A^*_{night} expressions are given in section 2.4.2).
(2) Calculated from Eq. (10) for GP 1 and from Eq. (11) for GP 2
(3) Calculated from Eq. (9)

Table 3. Summary table of data used calculated N isotopic fractionation between NO_x and NO_2: calculated A^*, calculated F_N, measured f_{NO_2}, calculated $\Delta(NO_2 - NO_x)$, measured $\delta^{15}N(NO_2)$, and calculated $\delta^{15}N(NO_x)$ (mean value ± absolute uncertainty).

4.3.1 NO_x emission sources

To identify the main source of NO_x that contributes to the calculated $\delta^{15}N(NO_x)$ values at our site, Figure 4 displays the temporal variation of $\delta^{15}N(NO_x)$ obtained from individual NO_2 samples (thick black line) and the $\delta^{15}N$ range for different NO_x emission sources (colored bands) such as for coal combustion ((19 ± 3) ‰; Felix et al., 2012; Elliott et al., 2019),

https://doi.org/10.5194/egusphere-2023-744
Preprint. Discussion started: 28 April 2023

biomass combustion ((–0.2 ± 0.3) ‰; Fibiger and Hastings, 2016; Martinelli et al., 1999), vehicle exhaust ((–7.3 ± 7.7) ‰; Zong et al., 2017), fossil gas combustion ((–15 ± 1.0) ‰; Walters et al., 2015), and fertilized soils ((–33.8 ± 12.2) ‰; Miller et al., 2018). It is important to stress that the literature is highly uncertain on assigning a consistent $\delta^{15}N$ value to vehicle exhaust, mainly because the value can vary depending on factors such as the type of fuel used, the type of vehicle, the presence of an emission control system, and the time of commuting (Ammann et al., 1999; Felix and Elliott, 2014; Heaton, 1990; Miller et al., 2017; Walters et al., 2015b; Zong et al., 2020, 2017). In this study, we use the mean vehicle-emitted $\delta^{15}N(NO_x)$ value given by Zong et al. (2017), which is derived from the integration of 151 measurements found in the literature.

As previously noted, the values of $\delta^{15}N(NO_x)$ show much less variability than $\delta^{15}N(NO_2)$, with no significant differences observed between daytime and nighttime values. The values of $\delta^{15}N(NO_x)$ range from −11.0 ‰ to −4.1 ‰ and, despite the associated uncertainty, they are consistent with the range of NO_x emissions from vehicle exhaust. The two sampling periods show similar $\delta^{15}N(NO_x)$ values with a slight diel variability. The estimated small variation in $\delta^{15}N(NO_x)$ throughout the day can be attributed to the temporal changes in the $\delta^{15}N$ signature of mobile NO_x sources. It has been shown that NO_x emitted by cold engines has a lower $\delta^{15}N$ signature compared to NO_x emitted from warm engines (Walters et al., 2015b). Hence, the early morning drop in $\delta^{15}N(NO_x)$ could be attributed to the influence of NO_x emitted from cold engines. As the day progresses and the time of commuting increases, daytime $\delta^{15}N(NO_x)$ values gradually increase. Conversely, during the night, the slow decline in $\delta^{15}N(NO_x)$ could be due to the removal of NO_x from vehicle exhaust by NO_x emitted by fossil gas combustion, which is commonly used for home heating.

According to local NO_x emissions inventories (Atmo-Auvergne-Rhône-Alpes, 2018; ORCAE, 2022), road transport is responsible of 64 % of NO_x emissions, ahead of heating oil and fossil gas combustion. Despite the consistency between our results and existing inventories, the significant variability in the $\delta^{15}N$ signature of NO_x emissions from vehicle exhaust preclude a reliable quantitative source apportionment of NO_x emissions from our estimated $\delta^{15}N(NO_x)$ values. Furthermore, the lack of information on the $\delta^{15}N$ signature of NO_x emitted from heating-oil combustion could add to the potential bias of an emission source apportionment.

https://doi.org/10.5194/egusphere-2023-744
Preprint. Discussion started: 28 April 2023

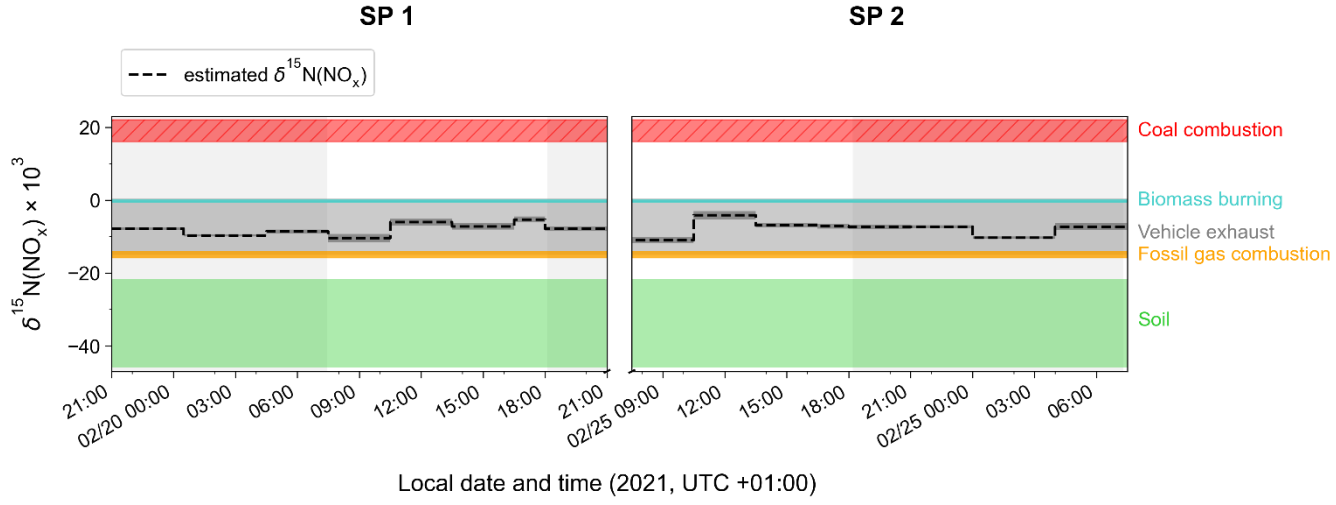

Figure 4. Time evolution of $\delta^{15}N(NO_x)$ (black solid line) estimated from $\delta^{15}N(NO_2)$ observations in Chamonix after correction of N fractionation effect (length of horizontal line = sampling period, black shaded area = overall calculation error bar). Coloured shaded areas represent the standard deviation of the mean $\delta^{15}N$ value of individual NO_x emission source (coal combustion in red, mean mobile source in grey, biomass burning in blue, fossil gas in orange, and soil emissions in green). Grey shaded areas represent the night duration

4.4 On the use of $\delta^{15}N(NO_3^-)$ observations

In the previous section, we demonstrated that there is a significant N partitioning between NO_x emissions and NO_2, with the latter being enriched in ^{15}N compared to NO_x emissions. An important ^{15}N enrichment is also observed in the $\delta^{15}N(NO_3^-)$ values, suggesting that the collected NO_3^- was mostly formed locally through the rapid conversion of NO_2.

At night during SP 1 and SP 2, $\delta^{15}N(NO_2)$ is close to $\delta^{15}N(NO_x)$ due to reduce N fractionation effects. However, nighttime NO_3^- is enriched in ^{15}N relative to NO_2 by +7.2 ‰ and +6.4 ‰ during SP 1 and SP 2, respectively (Table 4). If we assume that, at night, NO_3^- is formed by the conversion of surface NO_2 via the N_2O_5 pathway, then the difference between $\delta^{15}N(NO_3^-)$ and $\delta^{15}N(NO_2)$ ($\Delta^{15}(NO_3^- - NO_2)$) should reflect the N enrichment factor associated to this oxidation processes. During the night, it is likely that an isotopic equilibrium is established between NO_2, NO_3, and N_2O_5, which would affect the ^{15}N of NO_3^- produced at night (Walters and Michalski, 2016). According to the EIE fractionation faction between N_2O_5 and NO_2 (Walters and Michalski, 2015), and neglecting KIE associated with the N_2O_5 pathway, the isotopic composition of NO_3^- produced through this process should be enriched by around 29 ‰ (using the mean nighttime temperature at our site), which is about three times higher than observations. These results emphasize the significance of improving our understanding of ^{15}N fractionation between NO_2 and NO_3^- associated to the N_2O_5 pathway. This could be achieved by distinguishing individual processes using an atmospheric simulation chamber, which will be the subject of further investigation.

https://doi.org/10.5194/egusphere-2023-744
Preprint. Discussion started: 28 April 2023

During the day, the ^{15}N isotopic enrichment of NO_2 and NO_3^- shows a very contrasted distribution between SP 1 and SP 2, with a respective $\Delta^{15}(NO_3^- - NO_2)$ value of +1.4 ‰ and −15.0 ‰ (Table 4). Although subjected to significant uncertainties (Fan et al., 2019), the OH pathway is often associated to an KIE effect of −3 ‰ (Freyer, 1991), which is at odds with our observations. Similarly to the N_2O_5 pathway, there is an important need to better estimate the fractionation factor associate to the OH pathway. Nevertheless, the significant difference in $\Delta^{15}(NO_3^- - NO_2)$ between SP 1 and SP 2 provides further evidence that NO_3^- collected during the daytime of these two periods did not originate from the same sources.

	Day		*Night*	
	SP 1	SP 2	SP 1	SP 2
$\delta^{15}N(NO_2)^{(1)}$ /‰	7.7 ± 5.5	17.0 ± 13.0	−7.5 ± 1.3	−6.9 ± 2.5
$\delta^{15}N(NO_3^-)^{(2)}$ /‰	9.1 ± 8.0	2.0 ± 5.3	−0.3	−0.5
$\delta^{15}N(NO_x)^{(3)}$ /‰	−6.2 ± 1.0	−6.1 ± 1.7	−8.5 ± 0.9	−8.1 ± 1.5
$\Delta^{15}(NO_3^- - NO_2)$ /‰	1.4	−15.0	7.2	6.4

(1) Mean observed $\delta^{15}N(NO_2)$ between 7:30–16:30 LT for daytime and between 21:30–4:30 LT for nighttime
(2) Mean observed $\delta^{15}N(NO_3^-)$ between 10:30–18:00 LT for daytime and between 00:00–7:30 LT for nighttime
(3) Mean atmospheric $\delta^{15}N$ of NO_x between 7:30–18:30 LT for daytime and between 18:30–7:30 LT for nighttime

Table 4. Mean observed $\delta^{15}N$ data of NO_2 ($\delta^{15}N(NO_2)$) and NO_3^- ($\delta^{15}N(NO_3^-)$), calculated atmospheric $\delta^{15}N$ of NO_x ($\delta^{15}N(NO_x)$, and $\delta^{15}N$ shift of $\delta^{15}N(NO_3^-)$ relative to $\delta^{15}N(NO_x)$ ($\Delta^{15}(NO_3^- - NO_2)$).

5 Summary and implications

This study reports the first simultaneous measurements and analysis of $\Delta^{17}O$ and $\delta^{15}N$ in NO_2 and NO_3^-. The samplings were conducted at high temporal resolution (~ 3 h) in Chamonix, France. Over a two-day period in late February 2021, the isotopic signals of both NO_2 and NO_3^- show significant sub-daily variabilities.

The observed variability of $\Delta^{17}O(NO_2)$ is accurately constrained using $\Delta^{17}O$ mass balance equations and corroborate the analysis of previous observations. Sub-daily variability in the $NO_x/O_3/RO_2$ chemistry is detected, with estimates indicating pmol mol^{-1} level of RO_2 which contributed significantly to the formation of NO_2 in the early morning under high-NO_x conditions. Such effective production of radical species has been previously detected in other urban areas in wintertime. On average, the high levels of NO_2 at our site are primarily driven by local NO_x emissions undergoing O_3 oxidation. $\Delta^{17}O(NO_2)$ at night reveals substantial surface NO_x emissions. These results provide additional evidences that $\Delta^{17}O(NO_2)$ measurements represent valuable constraints in the study of the reactive NO_x chemistry, down to the sub-daily temporal

https://doi.org/10.5194/egusphere-2023-744
Preprint. Discussion started: 28 April 2023

scale. A clear linear relationship is found between $\delta^{15}N(NO_2)$ and the NO_2/NO_x ratio, indicating very significant post-emission N fractionation effects. The slope of this linear relationship is in very good agreement with the theoretical and laboratory estimates of N fractionation factors, which provides support for the current NO/NO_2 N isotopic fractionation theoretical framework. $\delta^{15}N(NO_2)$ values corrected for N fractionation dominated by equilibrium isotopic effects, indicate a major contribution from vehicle exhaust, which is consistent with local inventories.

$\Delta^{17}O$ and $\delta^{15}N$ of NO_3^- also exhibit significant variabilities at our site. Local $\Delta^{17}O$ mass balance equations of NO_3^-, constrained by observed $\Delta^{17}O(NO_2)$, suggest that, during the first day of sampling, NO_3^- was formed locally from the oxidation of NO_2 by OH radicals during the day, and via the heterogeneous hydrolysis of N_2O_5 during the night. The second day of sampling was affected by a Saharan dust event, followed by notable changes in the isotopic composition of NO_3^-. The formation of a nighttime inversion layer at the sampling site might influence the vertical distribution of $\Delta^{17}O(NO_2)$, resulting in a positive gradient of $\Delta^{17}O(NO_3^-)$ with altitude, independently of the NO_2 to NO_3^- conversion processes. In such scenario, the presence of Saharan dust can accelerate the dry deposition of the enriched NO_3^- formed aloft, which is then mixed with the NO_3^- formed at the surface when the inversion breaks up during the day. Although still uncertain, the influence of the boundary layer dynamics on the distribution of $\Delta^{17}O$ in NO_3^- should be investigated in the future, notably for urban areas in winter. $\delta^{15}N(NO_3^-)$ records need to be corrected from N fractionation effects if they are to be used to trace back accurately the $\delta^{15}N$ fingerprint of the NO_3^- sources. However, the combined analysis of the first concurrent observations of $\delta^{15}N$ in NO_2 and NO_3^- highlights persistent uncertainties in current estimates of the N fractionation factors associated with NO_2 to NO_3^- conversion processes. Detailed simulation chamber experiments could provide more kinetic data on the various N fractionation processes in order to exploit better $\delta^{15}N(NO_3^-)$ records in the identification and quantification of reactive nitrogen sources.

The present thorough investigation of the $\Delta^{17}O$ and $\delta^{15}N$ in NO_2 and NO_3^- highlights (1) the potential to use sub-daily $\Delta^{17}O$ and $\delta^{15}N$ records to trace the sources and formation chemistry of NO_3^-, (2) the importance of using observations of NO_2 isotopic composition to avoid misinterpretation of NO_3^- isotopic records, and (3) the persistent knowledge gaps that have so far prevented a complete picture of the factors that determine the variability of NO_3^- isotopic records. In most studies, the NO_3^- isotopic composition is interpreted on the basis of estimations on the isotopic composition of its precursor gases assuming that both the chemistry of NO_2 (including its conversion to NO_3^-) and isotopic fractionation effects are known. Given the recent development of a method for measuring the multi-isotopic composition of NO_2, it is important to test the accuracy and validity of the current interpretation isotopic framework of NO_3^-. Such investigations can be performed by collecting simultaneously NO_2 and NO_3^-, as done in this study. We recommend using this approach more frequently in order to avoid biased interpretation of NO_3^- isotopic records, particularly in urban areas during winter, and at high temporal resolution (<24 h). In addition, a focus should be given on the vertical distribution of NO_2 and NO_3^- isotopic composition.

https://doi.org/10.5194/egusphere-2023-744
Preprint. Discussion started: 28 April 2023

Appendix A: Reaction chemical rate

Reactions	Rate constants /cm^3 mol^{-1} s^{-1}	References
$NO + O_3 \rightarrow NO_2 + O_2$	$k_{NO+O_3} = 1.4 \times 10^{-12} \exp(-1310(K)/T)$	Atkinson et al. (2004)
$NO + RO_2 \rightarrow NO_2 + RO$	$k_{NO+RO_2} = 2.3 \times 10^{-12} \exp(360(K)//T)$	Atkinson et al. (2006)
$NO_2 + O_3 \xrightarrow{M} NO_3 + O_2$	$k_{NO_2+O_3} = 1.4 \times 10^{-13} \exp(-2470(K)//T)$	Atkinson et al. (2004)
$^{15}NO_2 + {}^{14}NO \rightarrow {}^{14}NO_2 + {}^{15}NO$	$k_{NO+NO_2} = 8.14 \times 10^{-14}$	Sharma et al. (1970)

Table A1. Kinetic constants used in this study.

Appendix B: Atmospheric lifetime of NO_2 and NO_3^-

	τ_{NO_2} (1)	$\tau_{NO_3^-}$ (2)	$k_{d(NO_2)}$ (s^{-1})	$k_{d(NO_3^-)}$ (s^{-1})
Day	5.1 min	27.8 h	0.5×10^{-5}	1.0×10^{-5}
Night	10.0 h	5.6 h	2.5×10^{-5}	5.0×10^{-5}

(1) Atmospheric lifetime relative to photolysis during the day (dry deposition and reaction NO_2 + OH are negligible) and to dry deposition and oxidation via O_3 during the night.
(2) Atmospheric lifetime relative to dry deposition
The boundary layer is fixed at 500 m during the day and at 100 m during the night. Dry deposition velocity (V_d) is fixed at 0.25 cm s^{-1} and 0.50 cm s^{-1} for NO_2 and NO_3^-, respectively (Holland et al., 1999; Zhang et al., 2009).

Table B1. Mean daytime (07:30–18:00 LT) and nighttime (18:00–07:30 LT) atmospheric lifetime of NO_2 (τ_{NO_2}) and NO_3^- ($\tau_{NO_3^-}$) and dry deposition constant ($k_d = V_d \times$ BLH where V_d is the dry deposition velocity and BLH is the boundary layer height).

https://doi.org/10.5194/egusphere-2023-744
Preprint. Discussion started: 28 April 2023

Appendix C: Schematic of the N reactive cycle and associated $\Delta^{17}O$ transfers and N enrichment factors

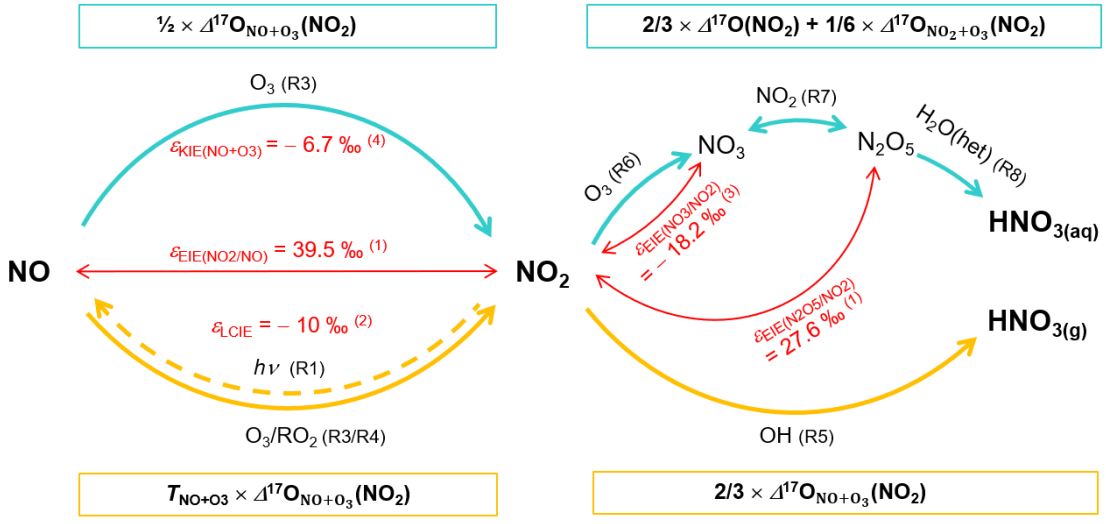

(1) Calculated at 298 K (Walters and Michalski, 2015)
(2) Experimental study at 298 K (Li et al., 2020)
(3) Calculated at 298 K (Walters et al., 2016)
(4) Calculated at 298 K (Fang et al., 2021)

Figure C1. Adapted from Elliott et al., (2019). Sketch of dominant daytime (thick yellow arrows) and nighttime (thick cyan arrows) NO_x to NO_3^- conversion processes and associated quantified N fractionation effects at 298 K (thin red arrows and text) and $\Delta^{17}O$ transfers (yellow and cyan boxes)

Appendix D: Equilibrium N fractionation factors

$$(\alpha_{EIE(X/Y)} - 1) \times 1000 = \frac{A}{T^4} \times 10^{10} + \frac{B}{T^3} \times 10^8 + \frac{C}{T^2} \times 10^6 + \frac{D}{T} \times 10^4$$

X/Y	A	B	C	D
NO_2/NO	3.847	–7.680	6.003	–0.118
N_2O_5/NO_2	1.004	–2.525	2.718	0.135

$$(\alpha_{KIE(X+Y)} - 1) \times 1000 = A \times exp(B/T)$$

X + Y	A	B
$NO + O_3$	0.982	3.352

Table D1. Calculated regression coefficients for the N isotope exchange between NO_2/NO and N_2O_5/NO_2 over the temperature range of 150 to 450 K (Walters and Michalski, 2015) and for the N kinetic fractionation for the reaction $NO + O_3$ over the temperature range of 220 to 320 K (Fang et al., 2021).

https://doi.org/10.5194/egusphere-2023-744
Preprint. Discussion started: 28 April 2023

Data availability

Data presented in this article are included in the Supplement.

Author contributions.

Grants obtained by KL and JS funded the project. AB, RB, QF, and IV performed the calibration of IBBCEAS and OFCEAS instruments, data acquisition and post-processing. SA conducted the sampling and laboratory analysis. NC provided technical support for isotopic mass spectrometry analysis. The study was designed as part of SA's PhD thesis supervised by SB and JS. The paper was written by SA under the supervision of JS and SB and contributions from all co-authors.

Competing interests.

The authors declare that they have no conflict of interest.

Acknowledgements.

This work benefited from CNRS and IGE infrastructures and laboratory platforms. The authors acknowledge the support of the CASPA program (Climate-relevant Aerosol Sources and Processes in the Arctic). The authors gratefully acknowledge Catherine Coulaud for providing temperature data in Chamonix, Jean-Luc Jaffrezo for providing data of previous filter measurements in Chamonix, and Anthony Lemoine, Matthieu Lafaysse and Louis Le Toumelin for providing S2M reanalysis and meteorological data. The authors particularly thanks Patrick Ginot, Anthony Vella, Armelle Crouzet, and Bruno Jourdain for instrumental and laboratory technical support. Finally, the authors thank Alexis Lamothe for assistance during the sampling campaign and Pete Akers for his thorough proofreading of the manuscript and his constructive comments.

Financial support.

This research has been supported by the Agence Nationale de la Recherche (ANR) via contract ANR-21-CE01-0017 CASPA and INSU-CNRS (National Institute of Sciences of the Universe) via its national LEFE program (Les Enveloppes Fluides et l'Environnement) and by a grant from Labex OSUG@2020 (Investissements d'avenir – ANR10 LABX56) and IDEX-UGA ANR project ANR-15-IDEX-02.

https://doi.org/10.5194/egusphere-2023-744
Preprint. Discussion started: 28 April 2023

References

Albertin, S., Savarino, J., Bekki, S., Barbero, A., and Caillon, N.: Measurement report: Nitrogen isotopes ($\delta^{15}N$) and first quantification of oxygen isotope anomalies ($\Delta^{17}O$, $\delta^{18}O$) in atmospheric nitrogen dioxide, Atmospheric Chemistry and Physics, 21, 10477–10497, https://doi.org/10.5194/acp-21-10477-2021, 2021.

Alexander, B., Savarino, J., Kreutz, K. J., and Thiemens, M. H.: Impact of preindustrial biomass-burning emissions on the oxidation pathways of tropospheric sulfur and nitrogen, Journal of Geophysical Research: Atmospheres, 109, https://doi.org/10.1029/2003JD004218, 2004.

Alexander, B., Hastings, M. G., Allman, D. J., Dachs, J., Thornton, J. A., and Kunasek, S. A.: Quantifying atmospheric nitrate formation pathways based on a global model of the oxygen isotopic composition ($\Delta^{17}O$) of atmospheric nitrate, Atmospheric Chemistry and Physics, 9, 5043–5056, https://doi.org/10.5194/acp-9-5043-2009, 2009.

Alexander, B., Sherwen, T., Holmes, C. D., Fisher, J. A., Chen, Q., Evans, M. J., and Kasibhatla, P.: Global inorganic nitrate production mechanisms: comparison of a global model with nitrate isotope observations, Atmospheric Chemistry and Physics, 20, 3859–3877, https://doi.org/10.5194/acp-20-3859-2020, 2020.

Alicke, B., Geyer, A., Hofzumahaus, A., Holland, F., Konrad, S., Pätz, H. W., Schäfer, J., Stutz, J., Volz-Thomas, A., and Platt, U.: OH formation by HONO photolysis during the BERLIOZ experiment, Journal of Geophysical Research: Atmospheres, 108, PHO 3-1-PHO 3-17, https://doi.org/10.1029/2001JD000579, 2003.

Allard, J.: Qualité de l'air dans la Vallée de l'Arve : météorologie locale et mesures des réductions des émissions liées au chauffage au bois, PhD Thesis, Université Grenoble Alpes, 2018.

Altieri, K. E., Burger, J., Language, B., and Piketh, S. J.: A case study in the wintertime Vaal Triangle Air-Shed Priority Area on the utility of the nitrogen stable isotopic composition of aerosol nitrate to identify NOx sources, Clean Air Journal, 32, https://doi.org/10.17159/caj/2022/32/1.12505, 2022.

Ammann, M., Siegwolf, R., Pichlmayer, F., Suter, M., Saurer, M., and Brunold, C.: Estimating the uptake of trafic-derived NO2 from 15N abundance in Norway spruce needles, Oecologia, 118, 124–131, https://doi.org/10.1007/s004420050710, 1999.

Angelisi, M. D. and Gaudichet, A.: Saharan dust deposition over Mont Blanc (French Alps) during the last 30 years, Tellus B, 43, 61–75, https://doi.org/10.1034/j.1600-0889.1991.00005.x, 1991.

Atkinson, R., Baulch, D. L., Cox, R. A., Crowley, J. N., Hampson, R. F., Hynes, R. G., Jenkin, M. E., Rossi, M. J., and Troe, J.: Evaluated kinetic and photochemical data for atmospheric chemistry: Volume I - gas phase reactions of O_x, HO_x, NO_x and SO_x species, Atmospheric Chemistry and Physics, 4, 1461–1738, https://doi.org/10.5194/acp-4-1461-2004, 2004.

Atkinson, R., Baulch, D. L., Cox, R. A., Crowley, J. N., Hampson, R. F., Hynes, R. G., Jenkin, M. E., Rossi, M. J., Troe, J., and IUPAC Subcommittee: Evaluated kinetic and photochemical data for atmospheric chemistry: Volume II - gas phase reactions of organic species, Atmospheric Chemistry and Physics, 6, 3625–4055, https://doi.org/10.5194/acp-6-3625-2006, 2006.

https://doi.org/10.5194/egusphere-2023-744
Preprint. Discussion started: 28 April 2023

Atmo-Auvergne-Rhône-Alpes: Bilan des connaissances sur la qualité de l'air dans la vallée de l'Arve, Atmo-Auvergne-Rhône-Alpes, 2018.

Aumont, B., Chervier, F., and Laval, S.: Contribution of HONO sources to the NOx/HOx/O3 chemistry in the polluted boundary layer, Atmospheric Environment, 37, 487–498, https://doi.org/10.1016/S1352-2310(02)00920-2, 2003.

Aymoz, G., Jaffrezo, J.-L., Jacob, V., Colomb, A., and George, C.: Evolution of organic and inorganic components of aerosol during a Saharan dust episode observed in the French Alps, Atmospheric Chemistry and Physics, 4, 2499–2512, https://doi.org/10.5194/acp-4-2499-2004, 2004.

Aymoz, G., Jaffrezo, J. L., Chapuis, D., Cozic, J., and Maenhaut, W.: Seasonal variation of PM_{10} main constituents in two valleys of the French Alps. I: EC/OC fractions, Atmospheric Chemistry and Physics, 7, 661–675, https://doi.org/10.5194/acp-7-661-2007, 2007.

Barbero, A., Blouzon, C., Savarino, J., Caillon, N., Dommergue, A., and Grilli, R.: A compact incoherent broadband cavity-enhanced absorption spectrometer for trace detection of nitrogen oxides, iodine oxide and glyoxal at levels below parts per billion for field applications, Atmospheric Measurement Techniques, 13, 4317–4331, https://doi.org/10.5194/amt-13-4317-2020, 2020.

Barkan, E. and Luz, B.: High-precision measurements of $^{17}O/^{16}O$ and $^{18}O/^{16}O$ of O_2 and O_2/Ar ratio in air, Rapid Commun. Mass Spectrom., 17, 2809–2814, https://doi.org/10.1002/rcm.1267, 2003.

Bauer, S. E., Koch, D., Unger, N., Metzger, S. M., Shindell, D. T., and Streets, D. G.: Nitrate aerosols today and in 2030: a global simulation including aerosols and tropospheric ozone, Atmos. Chem. Phys., 7, 5043–5059, https://doi.org/10.5194/acp-7-5043-2007, 2007.

Bekker, C., Walters, W. W., Murray, L. T., and Hastings, M. G.: Nitrate chemistry in the northeast US – Part 1: Nitrogen isotope seasonality tracks nitrate formation chemistry, Atmospheric Chemistry and Physics, 23, 4185–4201, https://doi.org/10.5194/acp-23-4185-2023, 2023.

Berhanu, T. A., Savarino, J., Bhattacharya, S. K., and Vicars, W. C.: ^{17} O excess transfer during the $NO_2 + O_3 \rightarrow NO_3 + O_2$ reaction, The Journal of Chemical Physics, 136, 044311, https://doi.org/10.1063/1.3666852, 2012.

Brown, S. S.: Variability in Nocturnal Nitrogen Oxide Processing and Its Role in Regional Air Quality, Science, 311, 67–70, https://doi.org/10.1126/science.1120120, 2006.

Brown, S. S. and Stutz, J.: Nighttime radical observations and chemistry, Chem Soc Rev, 41, 6405–6447, https://doi.org/10.1039/c2cs35181a, 2012.

Brulfert, G., Chemel, C., Chaxel, E., and Chollet, J. P.: Modelling photochemistry in alpine valleys, Atmos. Chem. Phys., 2005.

Casciotti, K. L., Sigman, D. M., Hastings, M. G., Böhlke, J. K., and Hilkert, A.: Measurement of the oxygen isotopic composition of nitrate in seawater and freshwater using the denitrifier method, Analytical Chemistry, 74, 4905–4912, https://doi.org/10.1021/ac020113w, 2002.

https://doi.org/10.5194/egusphere-2023-744
Preprint. Discussion started: 28 April 2023

Chang, Y., Zhang, Y., Tian, C., Zhang, S., Ma, X., Cao, F., Liu, X., Zhang, W., Kuhn, T., and Lehmann, M. F.: Nitrogen isotope fractionation during gas-to-particle conversion of NO_x to NO_3^- in the atmosphere – implications for isotope-based NO_x source apportionment, Atmospheric Chemistry and Physics, 18, 11647–11661, https://doi.org/10.5194/acp-18-11647-2018, 2018.

Chazette, P., Couvert, P., Randriamiarisoa, H., Sanak, J., Bonsang, B., Moral, P., Berthier, S., Salanave, S., and Toussaint, F.: Three-dimensional survey of pollution during winter in French Alps valleys, Atmospheric Environment, 39, 1035–1047, https://doi.org/10.1016/j.atmosenv.2004.10.014, 2005.

Crutzen, P. J.: The Role of NO and NO $_2$ in the Chemistry of the Troposphere and Stratosphere, Annu. Rev. Earth Planet. Sci., 7, 443–472, https://doi.org/10.1146/annurev.ea.07.050179.002303, 1979.

Delmas, R. J.: Snow chemistry of high altitude glaciers in the French Alps, 46, 304, https://doi.org/10.3402/tellusb.v46i4.15806, 1994.

Dentener, F. J. and Crutzen, P. J.: Reaction of N2O5 on tropospheric aerosols: Impact on the global distributions of NO x , O3, and OH, Journal of Geophysical Research: Atmospheres, 98, 7149–7163, https://doi.org/10.1029/92JD02979, 1993.

Di Mauro, B., Garzonio, R., Rossini, M., Filippa, G., Pogliotti, P., Galvagno, M., Morra di Cella, U., Migliavacca, M., Baccolo, G., Clemenza, M., Delmonte, B., Maggi, V., Dumont, M., Tuzet, F., Lafaysse, M., Morin, S., Cremonese, E., and Colombo, R.: Saharan dust events in the European Alps: role in snowmelt and geochemical characterization, The Cryosphere, 13, 1147–1165, https://doi.org/10.5194/tc-13-1147-2019, 2019.

Dubey, M. K., Mohrschladt, R., Donahue, N. M., and Anderson, J. G.: Isotope Specific Kinetics of Hydroxyl Radical (OH) with Water (H2O): Testing Models of Reactivity and Atmospheric Fractionation, J. Phys. Chem. A, 101, 1494–1500, https://doi.org/10.1021/jp962332p, 1997.

Elliott, E. M., Kendall, C., Wankel, S. D., Burns, D. A., Boyer, E. W., Harlin, K., Bain, D. J., and Butler, T. J.: Nitrogen Isotopes as Indicators of NOx Source Contributions to Atmospheric Nitrate Deposition Across the Midwestern and Northeastern United States, Environ. Sci. Technol., 41, 7661–7667, https://doi.org/10.1021/es070898t, 2007.

Elliott, E. M., Yu, Z., Cole, A. S., and Coughlin, J. G.: Isotopic advances in understanding reactive nitrogen deposition and atmospheric processing, Science of The Total Environment, 662, 393–403, https://doi.org/10.1016/j.scitotenv.2018.12.177, 2019.

Emmerson, K. M., Carslaw, N., Carpenter, L. J., Heard, D. E., Lee, J. D., and Pilling, M. J.: Urban Atmospheric Chemistry During the PUMA Campaign 1: Comparison of Modelled OH and HO2 Concentrations with Measurements, J Atmos Chem, 52, 143–164, https://doi.org/10.1007/s10874-005-1322-3, 2005.

Erbland, J., Vicars, W. C., Savarino, J., Morin, S., Frey, M. M., Frosini, D., Vince, E., and Martins, J. M. F.: Air–snow transfer of nitrate on the East Antarctic Plateau – Part 1: Isotopic evidence for a photolytically driven dynamic equilibrium in summer, Atmos. Chem. Phys., 13, 6403–6419, https://doi.org/10.5194/acp-13-6403-2013, 2013.

https://doi.org/10.5194/egusphere-2023-744
Preprint. Discussion started: 28 April 2023

Fan, M.-Y., Zhang, Y.-L., Lin, Y.-C., Chang, Y.-H., Cao, F., Zhang, W.-Q., Hu, Y.-B., Bao, M.-Y., Liu, X.-Y., Zhai, X.-Y., Lin, X., Zhao, Z.-Y., and Song, W.-H.: Isotope-based source apportionment of nitrogen-containing aerosols: A case study in an industrial city in China, Atmospheric Environment, 212, 96–105, https://doi.org/10.1016/j.atmosenv.2019.05.020, 2019.

Fan, M.-Y., Zhang, Y.-L., Lin, Y.-C., Hong, Y., Zhao, Z.-Y., Xie, F., Du, W., Cao, F., Sun, Y., and Fu, P.: Important Role of NO3 Radical to Nitrate Formation Aloft in Urban Beijing: Insights from Triple Oxygen Isotopes Measured at the Tower, Environ. Sci. Technol., 56, 6870–6879, https://doi.org/10.1021/acs.est.1c02843, 2022.

Fan, M.-Y., Zhang, W., Zhang, Y.-L., Li, J., Fang, H., Cao, F., Yan, M., Hong, Y., Guo, H., and Michalski, G.: Formation Mechanisms and Source Apportionments of Nitrate Aerosols in a Megacity of Eastern China Based On Multiple Isotope Observations, Journal of Geophysical Research: Atmospheres, 128, e2022JD038129, https://doi.org/10.1029/2022JD038129, 2023.

Fang, H., Walters, W. W., Mase, D., and Michalski, G.: i_NRACM: incorporating ^{15}N into the Regional Atmospheric Chemistry Mechanism (RACM) for assessing the role photochemistry plays in controlling the isotopic composition of NO_x, NO_y, and atmospheric nitrate, Geoscientific Model Development, 14, 5001–5022, https://doi.org/10.5194/gmd-14-5001-2021, 2021.

Felix, J. D. and Elliott, E. M.: Isotopic composition of passively collected nitrogen dioxide emissions: Vehicle, soil and livestock source signatures, Atmospheric Environment, 92, 359–366, https://doi.org/10.1016/j.atmosenv.2014.04.005, 2014.

Felix, J. D., Elliott, E. M., and Shaw, S. L.: Nitrogen Isotopic Composition of Coal-Fired Power Plant NOx: Influence of Emission Controls and Implications for Global Emission Inventories, Environ. Sci. Technol., 46, 3528–3535, https://doi.org/10.1021/es203355v, 2012.

Fibiger, D. L. and Hastings, M. G.: First Measurements of the Nitrogen Isotopic Composition of NOx from Biomass Burning, Environ. Sci. Technol., 50, 11569–11574, https://doi.org/10.1021/acs.est.6b03510, 2016.

Finlayson-Pitts, B. J. and Pitts, J. N.: Chemistry of the Upper and Lower Atmosphere, Elsevier, https://doi.org/10.1016/B978-012257060-5/50003-4, 2000.

Frey, M. M., Savarino, J., Morin, S., Erbland, J., and Martins, J. M. F.: Photolysis imprint in the nitrate stable isotope signal in snow and atmosphere of East Antarctica and implications for reactive nitrogen cycling, Atmospheric Chemistry and Physics, 9, 8681–8696, https://doi.org/10.5194/acp-9-8681-2009, 2009.

Freyer, H. D.: Seasonal variation of 15N/14N ratios in atmospheric nitrate species, Tellus B, 43, 30–44, https://doi.org/10.1034/j.1600-0889.1991.00003.x, 1991.

Freyer, H. D., Kley, D., Volz-Thomas, A., and Kobel, K.: On the interaction of isotopic exchange processes with photochemical reactions in atmospheric oxides of nitrogen, Journal of Geophysical Research: Atmospheres, 98, 14791–14796, https://doi.org/10.1029/93JD00874, 1993.

https://doi.org/10.5194/egusphere-2023-744
Preprint. Discussion started: 28 April 2023

Galeazzo, T., Bekki, S., Martin, E., Savarino, J., and Arnold, S. R.: Photochemical box modelling of volcanic SO_2 oxidation: isotopic constraints, Atmospheric Chemistry and Physics, 18, 17909–17931, https://doi.org/10.5194/acp-18-17909-2018, 2018.

Galloway, J. N., Townsend, A. R., Erisman, J. W., Bekunda, M., Cai, Z., Freney, J. R., Martinelli, L. A., Seitzinger, S. P., and Sutton, M. A.: Transformation of the Nitrogen Cycle: Recent Trends, Questions, and Potential Solutions, Science, 320, 889–892, https://doi.org/10.1126/science.1136674, 2008.

Gaudel, A., Cooper, O. R., Ancellet, G., Barret, B., Boynard, A., Burrows, J. P., Clerbaux, C., Coheur, P.-F., Cuesta, J., Cuevas, E., Doniki, S., Dufour, G., Ebojie, F., Foret, G., Garcia, O., Granados-Muñoz, M. J., Hannigan, J. W., Hase, F., Hassler, B., Huang, G., Hurtmans, D., Jaffe, D., Jones, N., Kalabokas, P., Kerridge, B., Kulawik, S., Latter, B., Leblanc, T., Le Flochmoën, E., Lin, W., Liu, J., Liu, X., Mahieu, E., McClure-Begley, A., Neu, J. L., Osman, M., Palm, M., Petetin, H., Petropavlovskikh, I., Querel, R., Rahpoe, N., Rozanov, A., Schultz, M. G., Schwab, J., Siddans, R., Smale, D., Steinbacher, M., Tanimoto, H., Tarasick, D. W., Thouret, V., Thompson, A. M., Trickl, T., Weatherhead, E., Wespes, C., Worden, H. M., Vigouroux, C., Xu, X., Zeng, G., and Ziemke, J.: Tropospheric Ozone Assessment Report: Present-day distribution and trends of tropospheric ozone relevant to climate and global atmospheric chemistry model evaluation, Elementa: Science of the Anthropocene, 6, https://doi.org/10.1525/elementa.291, 2018.

Geng, L., Alexander, B., Cole-Dai, J., Steig, E. J., Savarino, J., Sofen, E. D., and Schauer, A. J.: Nitrogen isotopes in ice core nitrate linked to anthropogenic atmospheric acidity change, Proc. Natl. Acad. Sci. U.S.A., 111, 5808–5812, https://doi.org/10.1073/pnas.1319441111, 2014.

Geng, L., Murray, L. T., Mickley, L. J., Lin, P., Fu, Q., Schauer, A. J., and Alexander, B.: Isotopic evidence of multiple controls on atmospheric oxidants over climate transitions, Nature, 546, 133–136, https://doi.org/10.1038/nature22340, 2017.

Goudie, A. S. and Middleton, N. J.: Saharan dust storms: nature and consequences, Earth-Science Reviews, 56, 179–204, https://doi.org/10.1016/S0012-8252(01)00067-8, 2001.

Grannas, A. M., Jones, A. E., Dibb, J., Ammann, M., Anastasio, C., Beine, H. J., Bergin, M., Bottenheim, J., Boxe, C. S., Carver, G., Chen, G., Crawford, J. H., Dominé, F., Frey, M. M., Guzmán, M. I., Heard, D. E., Helmig, D., Hoffmann, M. R., Honrath, R. E., Huey, L. G., Hutterli, M., Jacobi, H. W., Klán, P., Lefer, B., McConnell, J., Plane, J., Sander, R., Savarino, J., Shepson, P. B., Simpson, W. R., Sodeau, J. R., von Glasow, R., Weller, R., Wolff, E. W., and Zhu, T.: An overview of snow photochemistry: evidence, mechanisms and impacts, Atmospheric Chemistry and Physics, 7, 4329–4373, https://doi.org/10.5194/acp-7-4329-2007, 2007.

Greilinger, M., Schauer, G., Baumann-Stanzer, K., Skomorowski, P., Schöner, W., and Kasper-Giebl, A.: Contribution of Saharan Dust to Ion Deposition Loads of High Alpine Snow Packs in Austria (1987–2017), Frontiers in Earth Science, 6, 2018.

Gu, P., Dallmann, T. R., Li, H. Z., Tan, Y., and Presto, A. A.: Quantifying Urban Spatial Variations of Anthropogenic VOC Concentrations and Source Contributions with a Mobile Sampling Platform, Int J Environ Res Public Health, 16, https://doi.org/10.3390/ijerph16091632, 2019.

https://doi.org/10.5194/egusphere-2023-744
Preprint. Discussion started: 28 April 2023

Hastings, M. G., Jarvis, J. C., and Steig, E. J.: Anthropogenic Impacts on Nitrogen Isotopes of Ice-Core Nitrate, Science, 324, 1288–1288, https://doi.org/10.1126/science.1170510, 2009.

He, P., Xie, Z., Chi, X., Yu, X., Fan, S., Kang, H., Liu, C., and Zhan, H.: Atmospheric $\Delta^{17}O(NO_3^-)$ reveals nocturnal chemistry dominates nitrate production in Beijing haze, Atmospheric Chemistry and Physics, 18, 14465–14476, https://doi.org/10.5194/acp-18-14465-2018, 2018.

He, P., Xie, Z., Yu, X., Wang, L., Kang, H., and Yue, F.: The observation of isotopic compositions of atmospheric nitrate in Shanghai China and its implication for reactive nitrogen chemistry, Science of The Total Environment, 714, 136727, https://doi.org/10.1016/j.scitotenv.2020.136727, 2020.

Heaton, T. H. E.: 15N/14N ratios of NOx from vehicle engines and coal-fired power stations, Tellus B, 42, 304–307, https://doi.org/10.1034/j.1600-0889.1990.00007.x-i1, 1990.

Hoesly, R. M., Smith, S. J., Feng, L., Klimont, Z., Janssens-Maenhout, G., Pitkanen, T., Seibert, J. J., Vu, L., Andres, R. J., Bolt, R. M., Bond, T. C., Dawidowski, L., Kholod, N., Kurokawa, J., Li, M., Liu, L., Lu, Z., Moura, M. C. P., O'Rourke, P. R., and Zhang, Q.: Historical (1750–2014) anthropogenic emissions of reactive gases and aerosols from the Community Emissions Data System (CEDS), Geoscientific Model Development, 11, 369–408, https://doi.org/10.5194/gmd-11-369-2018, 2018.

Holland, E. A., Dentener, F. J., Braswell, B. H., and Sulzman, J. M.: Contemporary and pre-industrial global reactive nitrogen budgets, Biogeochemistry, 46, 7–43, https://doi.org/10.1023/A:1006148011944, 1999.

Huang, R.-J., Zhang, Y., Bozzetti, C., Ho, K.-F., Cao, J.-J., Han, Y., Daellenbach, K. R., Slowik, J. G., Platt, S. M., Canonaco, F., Zotter, P., Wolf, R., Pieber, S. M., Bruns, E. A., Crippa, M., Ciarelli, G., Piazzalunga, A., Schwikowski, M., Abbaszade, G., Schnelle-Kreis, J., Zimmermann, R., An, Z., Szidat, S., Baltensperger, U., Haddad, I. E., and Prévôt, A. S. H.: High secondary aerosol contribution to particulate pollution during haze events in China, Nature, 514, 218–222, https://doi.org/10.1038/nature13774, 2014.

IPCC: Climate Change 2021 The Physical Science Basis Working Group I Contribution to the Sixth Assessment Report of the Intergovernmental Panel on Climate Change, 2021.

Johnston, J. C. and Thiemens, M. H.: The isotopic composition of tropospheric ozone in three environments, J. Geophys. Res., 102, 25395–25404, 1997.

Kaiser, J., Hastings, M. G., Houlton, B. Z., Röckmann, T., and Sigman, D. M.: Triple oxygen isotope analysis of nitrate using the denitrifier method and thermal decomposition of N_2O, Anal. Chem., 79, 599–607, https://doi.org/10.1021/ac061022s, 2007.

Kanaya, Y., Cao, R., Akimoto, H., Fukuda, M., Komazaki, Y., Yokouchi, Y., Koike, M., Tanimoto, H., Takegawa, N., and Kondo, Y.: Urban photochemistry in central Tokyo: 1. Observed and modeled OH and HO2 radical concentrations during the winter and summer of 2004, Journal of Geophysical Research: Atmospheres, 112, https://doi.org/10.1029/2007JD008670, 2007.

https://doi.org/10.5194/egusphere-2023-744
Preprint. Discussion started: 28 April 2023

Karydis, V. A., Tsimpidi, A. P., Pozzer, A., Astitha, M., and Lelieveld, J.: Effects of mineral dust on global atmospheric nitrate concentrations, Atmospheric Chemistry and Physics, 16, 1491–1509, https://doi.org/10.5194/acp-16-1491-2016, 2016.

Kirchstetter, T. W., Harley, R. A., and Littlejohn, D.: Measurement of Nitrous Acid in Motor Vehicle Exhaust, Environ. Sci. Technol., 30, 2843–2849, https://doi.org/10.1021/es960135y, 1996.

Krankowsky, D., Bartecki, F., Klees, G. G., Mauersberger, K., Schellenbach, K., and Stehr, J.: Measurement of heavy isotope enrichment in tropospheric ozone, Geophys. Res. Lett., 22, 1713–1716, 1995.

Kurtenbach, R., Becker, K. H., Gomes, J. A. G., Kleffmann, J., Lörzer, J. C., Spittler, M., Wiesen, P., Ackermann, R., Geyer, A., and Platt, U.: Investigations of emissions and heterogeneous formation of HONO in a road traffic tunnel, Atmospheric Environment, 35, 3385–3394, https://doi.org/10.1016/S1352-2310(01)00138-8, 2001.

Leighton, P. A.: Photochemistry of Air Pollution., 66, 1961.

Li, J., Zhang, X., Orlando, J., Tyndall, G., and Michalski, G.: Quantifying the nitrogen isotope effects during photochemical equilibrium between NO and NO_2: implications for $\delta^{15}N$ in tropospheric reactive nitrogen, Atmospheric Chemistry and Physics, 20, 9805–9819, https://doi.org/10.5194/acp-20-9805-2020, 2020.

Li, J., Davy, P., Harvey, M., Katzman, T., Mitchell, T., and Michalski, G.: Nitrogen isotopes in nitrate aerosols collected in the remote marine boundary layer: Implications for nitrogen isotopic fractionations among atmospheric reactive nitrogen species, Atmospheric Environment, 245, 118028, https://doi.org/10.1016/j.atmosenv.2020.118028, 2021.

Li, Y., Shi, G., Chen, Z., Lan, M., Ding, M., Li, Z., and Hastings, M. G.: Significant Latitudinal Gradient of Nitrate Production in the Marine Atmospheric Boundary Layer of the Northern Hemisphere, Geophysical Research Letters, 49, e2022GL100503, https://doi.org/10.1029/2022GL100503, 2022a.

Li, Z., Walters, W. W., Hastings, M. G., Song, L., Huang, S., Zhu, F., Liu, D., Shi, G., Li, Y., and Fang, Y.: Atmospheric nitrate formation pathways in urban and rural atmosphere of Northeast China: Implications for complicated anthropogenic effects, Environmental Pollution, 296, 118752, https://doi.org/10.1016/j.envpol.2021.118752, 2022b.

Lim, S., Lee, M., Savarino, J., and Laj, P.: Oxidation pathways and emission sources of atmospheric particulate nitrate in Seoul: based on $\delta^{15}N$ and $\Delta^{17}O$ measurements, Atmospheric Chemistry and Physics, 22, 5099–5115, https://doi.org/10.5194/acp-22-5099-2022, 2022.

Liu, J., Liu, Z., Ma, Z., Yang, S., Yao, D., Zhao, S., Hu, B., Tang, G., Sun, J., Cheng, M., Xu, Z., and Wang, Y.: Detailed budget analysis of HONO in Beijing, China: Implication on atmosphere oxidation capacity in polluted megacity, Atmospheric Environment, 244, 117957, https://doi.org/10.1016/j.atmosenv.2020.117957, 2021.

Liu, Z., Hu, K., Zhang, K., Zhu, S., Wang, M., and Li, L.: VOCs sources and roles in O3 formation in the central Yangtze River Delta region of China, Atmospheric Environment, 302, 119755, https://doi.org/10.1016/j.atmosenv.2023.119755, 2023.

Luo, L., Wu, S., Zhang, R., Wu, Y., Li, J., and Kao, S.: What controls aerosol δ15N-NO3−? NOx emission sources vs. nitrogen isotope fractionation, Science of The Total Environment, 871, 162185, https://doi.org/10.1016/j.scitotenv.2023.162185, 2023.

Martinelli, L. A., Piccolo, M. C., Townsend, A. R., Vitousek, P. M., Cuevas, E., McDowell, W., Robertson, G. P., Santos, O. C., and Treseder, K.: Nitrogen stable isotopic composition of leaves and soil: Tropical versus temperate forests, Biogeochemistry, 46, 45–65, https://doi.org/10.1023/A:1006100128782, 1999.

Mayer, H.: Air pollution in cities, Atmospheric Environment, 33, 4029–4037, https://doi.org/10.1016/S1352-2310(99)00144-2, 1999.

McCabe, J. R., Thiemens, M. H., and Savarino, J.: A record of ozone variability in South Pole Antarctic snow: Role of nitrate oxygen isotopes, Journal of Geophysical Research, 112, https://doi.org/10.1029/2006JD007822, 2007.

McIlvin, M. R. and Altabet, M. A.: Chemical Conversion of Nitrate and Nitrite to Nitrous Oxide for Nitrogen and Oxygen Isotopic Analysis in Freshwater and Seawater, Analytical Chemistry, 77, 5589–5595, https://doi.org/10.1021/ac050528s, 2005.

Michalski, G., Scott, Z., Kabiling, M., and Thiemens, M. H.: First measurements and modeling of $\Delta^{17}O$ in atmospheric nitrate., Geophysical Research Letters, 30, 1870, https://doi.org/10.1029/2003GL017015, 2003.

Michalski, G., Bhattacharya, S. K., and Girsch, G.: NO_x cycle and the tropospheric ozone isotope anomaly: an experimental investigation, Atmospheric Chemistry and Physics, 14, 4935–4953, https://doi.org/10.5194/acp-14-4935-2014, 2014.

Michoud, V., Doussin, J.-F., Colomb, A., Afif, C., Borbon, A., Camredon, M., Aumont, B., Legrand, M., and Beekmann, M.: Strong HONO formation in a suburban site during snowy days, Atmospheric Environment, 116, 155–158, https://doi.org/10.1016/j.atmosenv.2015.06.040, 2015.

Miller, D. J., Wojtal, P. K., Clark, S. C., and Hastings, M. G.: Vehicle NO_x emission plume isotopic signatures: Spatial variability across the eastern United States, Journal of Geophysical Research: Atmospheres, 122, 4698–4717, https://doi.org/10.1002/2016JD025877, 2017.

Miller, D. J., Chai, J., Guo, F., Dell, C. J., Karsten, H., and Hastings, M. G.: Isotopic Composition of In Situ Soil NO_x Emissions in Manure-Fertilized Cropland, Geophysical Research Letters, 45, 12,058-12,066, https://doi.org/10.1029/2018GL079619, 2018.

Morin, S., Savarino, J., Bekki, S., Gong, S., and Bottenheim, J. W.: Signature of Arctic surface ozone depletion events in the isotope anomaly ($\Delta^{17}O$) of atmospheric nitrate, Atmos. Chem. Phys., 7, 1451–1469, https://doi.org/10.5194/acp-7-1451-2007, 2007.

Morin, S., Savarino, J., Frey, M. M., Yan, N., Bekki, S., Bottenheim, J. W., and Martins, J. M. F.: Tracing the Origin and Fate of NOx in the Arctic Atmosphere Using Stable Isotopes in Nitrate, Science, 322, 730–732, https://doi.org/10.1126/science.1161910, 2008.

https://doi.org/10.5194/egusphere-2023-744
Preprint. Discussion started: 28 April 2023

Morin, S., Savarino, J., Frey, M. M., Domine, F., Jacobi, H.-W., Kaleschke, L., and Martins, J. M. F.: Comprehensive isotopic composition of atmospheric nitrate in the Atlantic Ocean boundary layer from 65°S to 79°N, Journal of Geophysical Research: Atmospheres, 114, https://doi.org/10.1029/2008JD010696, 2009.

Newsome, B. and Evans, M.: Impact of uncertainties in inorganic chemical rate constants on tropospheric composition and ozone radiative forcing, Atmos. Chem. Phys., 17, 14333–14352, https://doi.org/10.5194/acp-17-14333-2017, 2017.

ORCAE: Rapport des profils climat air énergie de la communauté de communes de la Vallée de Chamonix-Mont-Blanc, 2022.

Park, R. J., Jacob, D. J., Field, B. D., Yantosca, R. M., and Chin, M.: Natural and transboundary pollution influences on sulfate-nitrate-ammonium aerosols in the United States: Implications for policy, Journal of Geophysical Research: Atmospheres, 109, https://doi.org/10.1029/2003JD004473, 2004.

Penkett, S. A., Burgess, R. A., Coe, H., Coll, I., Hov, Ø., Lindskog, A., Schmidbauer, N., Solberg, S., Roemer, M., Thijsse, T., Beck, J., and Reeves, C. E.: Evidence for large average concentrations of the nitrate radical (NO3) in Western Europe from the HANSA hydrocarbon database, Atmospheric Environment, 41, 3465–3478, https://doi.org/10.1016/j.atmosenv.2006.11.055, 2007.

Pugh, T. A. M., Cain, M., Methven, J., Wild, O., Arnold, S. R., Real, E., Law, K. S., Emmerson, K. M., Owen, S. M., Pyle, J. A., Hewitt, C. N., and MacKenzie, A. R.: A Lagrangian model of air-mass photochemistry and mixing using a trajectory ensemble: the Cambridge Tropospheric Trajectory model of Chemistry And Transport (CiTTyCAT) version 4.2, Geosci. Model Dev., 5, 193–221, https://doi.org/10.5194/gmd-5-193-2012, 2012.

Quimbayo-Duarte, J., Chemel, C., Staquet, C., Troude, F., and Arduini, G.: Drivers of severe air pollution events in a deep valley during wintertime: A case study from the Arve river valley, France, Atmospheric Environment, 247, 118030, https://doi.org/10.1016/j.atmosenv.2020.118030, 2021.

Ren, X., Brune, W. H., Mao, J., Mitchell, M. J., Lesher, R. L., Simpas, J. B., Metcalf, A. R., Schwab, J. J., Cai, C., Li, Y., Demerjian, K. L., Felton, H. D., Boynton, G., Adams, A., Perry, J., He, Y., Zhou, X., and Hou, J.: Behavior of OH and HO_2 in the winter atmosphere in New York City, Atmospheric Environment, 40, 252–263, https://doi.org/10.1016/j.atmosenv.2005.11.073, 2006.

Richard, L., Romanini, D., and Ventrillard, I.: Nitric Oxide Analysis Down to ppt Levels by Optical-Feedback Cavity-Enhanced Absorption Spectroscopy, Sensors, 18, 1997, https://doi.org/10.3390/s18071997, 2018.

Savard, M. M., Cole, A. S., Vet, R., and Smirnoff, A.: The $\Delta^{17}O$ and $\delta^{18}O$ values of atmospheric nitrates simultaneously collected downwind of anthropogenic sources – implications for polluted air masses, Atmospheric Chemistry and Physics, 18, 10373–10389, https://doi.org/10.5194/acp-18-10373-2018, 2018.

Savarino, J., Bhattacharya, S. K., Morin, S., Baroni, M., and Doussin, J.-F.: The $NO+O_3$ reaction: A triple oxygen isotope perspective on the reaction dynamics and atmospheric implications for the transfer of the ozone isotope anomaly, J. Chem. Phys., 128, 194303, https://doi.org/10.1063/1.2917581, 2008.

https://doi.org/10.5194/egusphere-2023-744
Preprint. Discussion started: 28 April 2023

Savarino, J., Morin, S., Erbland, J., Grannec, F., Patey, M. D., Vicars, W., Alexander, B., and Achterberg, E. P.: Isotopic composition of atmospheric nitrate in a tropical marine boundary layer, PNAS, 110, 17668–17673, https://doi.org/10.1073/pnas.1216639110, 2013.

Savarino, J., Vicars, W. C., Legrand, M., Preunkert, S., Jourdain, B., Frey, M. M., Kukui, A., Caillon, N., and Roca, J. G.: Oxygen isotope mass balance of atmospheric nitrate at Dome C, East Antarctica, during the OPALE campaign, Atmos. Chem. Phys., 16, 2016.

Schwikowski, M., Seibert, P., Baltensperger, U., and Gaggeler, H. W.: A study of an outstanding Saharan dust event at the high-alpine site Jungfraujoch, Switzerland, Atmospheric Environment, 29, 1829–1842, https://doi.org/10.1016/1352-2310(95)00060-C, 1995.

Shah, V., Jaeglé, L., Thornton, J. A., Lopez-Hilfiker, F. D., Lee, B. H., Schroder, J. C., Campuzano-Jost, P., Jimenez, J. L., Guo, H., Sullivan, A. P., Weber, R. J., Green, J. R., Fiddler, M. N., Bililign, S., Campos, T. L., Stell, M., Weinheimer, A. J., Montzka, D. D., and Brown, S. S.: Chemical feedbacks weaken the wintertime response of particulate sulfate and nitrate to emissions reductions over the eastern United States, Proc Natl Acad Sci USA, 115, 8110–8115, https://doi.org/10.1073/pnas.1803295115, 2018.

Sharma, H. D., Jervis, R. E., and Wong, K. Y.: Isotopic exchange reactions in nitrogen oxides, J. Phys. Chem., 74, 923–933, https://doi.org/10.1021/j100699a044, 1970.

Sigman, D. M., Casciotti, K. L., Andreani, M., Barford, C., Galanter, M., and Böhlke, J. K.: A Bacterial Method for the Nitrogen Isotopic Analysis of Nitrate in Seawater and Freshwater, Analytical Chemistry, 73, 4145–4153, https://doi.org/10.1021/ac010088e, 2001.

Simpson, W. R., Brown, S. S., Saiz-Lopez, A., Thornton, J. A., and von Glasow, R.: Tropospheric Halogen Chemistry: Sources, Cycling, and Impacts, Chem. Rev., 115, 4035–4062, https://doi.org/10.1021/cr5006638, 2015.

Sodemann, H., Palmer, A. S., Schwierz, C., Schwikowski, M., and Wernli, H.: The transport history of two Saharan dust events archived in an Alpine ice core, Atmospheric Chemistry and Physics, 6, 667–688, https://doi.org/10.5194/acp-6-667-2006, 2006.

Stone, D., Whalley, L. K., and Heard, D. E.: Tropospheric OH and HO2 radicals: field measurements and model comparisons, Chem. Soc. Rev., 41, 6348–6404, https://doi.org/10.1039/C2CS35140D, 2012.

Tan, Z., Rohrer, F., Lu, K., Ma, X., Bohn, B., Broch, S., Dong, H., Fuchs, H., Gkatzelis, G. I., Hofzumahaus, A., Holland, F., Li, X., Liu, Y., Liu, Y., Novelli, A., Shao, M., Wang, H., Wu, Y., Zeng, L., Hu, M., Kiendler-Scharr, A., Wahner, A., and Zhang, Y.: Wintertime photochemistry in Beijing: observations of RO_x radical concentrations in the North China Plain during the BEST-ONE campaign, Atmos. Chem. Phys., 18, 12391–12411, https://doi.org/10.5194/acp-18-12391-2018, 2018.

Thiemens, M. H.: History and Applications of Mass-independent Isotope Effects, Annual Review of Earth and Planetary Sciences, 34, 217–262, https://doi.org/10.1146/annurev.earth.34.031405.125026, 2006.

https://doi.org/10.5194/egusphere-2023-744
Preprint. Discussion started: 28 April 2023

Tsimpidi, A. P., Karydis, V. A., and Pandis, S. N.: Response of Fine Particulate Matter to Emission Changes of Oxides of Nitrogen and Anthropogenic Volatile Organic Compounds in the Eastern United States, Journal of the Air & Waste Management Association, 58, 1463–1473, https://doi.org/10.3155/1047-3289.58.11.1463, 2008.

Usher, C. R., Michel, A. E., and Grassian, V. H.: Reactions on Mineral Dust, Chem. Rev., 103, 4883–4940, https://doi.org/10.1021/cr020657y, 2003.

Vicars, W. C. and Savarino, J.: Quantitative constraints on the ^{17}O-excess (Δ^{17}O) signature of surface ozone: Ambient measurements from 50°N to 50°S using the nitrite-coated filter technique, Geochimica et Cosmochimica Acta, 135, 270–287, https://doi.org/10.1016/j.gca.2014.03.023, 2014.

Vicars, W. C., Bhattacharya, S. K., Erbland, J., and Savarino, J.: Measurement of the 17O-excess (Δ17O) of tropospheric ozone using a nitrite-coated filter, Rapid Communications in Mass Spectrometry, 26, 1219–1231, https://doi.org/10.1002/rcm.6218, 2012.

Vicars, W. C., Morin, S., Savarino, J., Wagner, N. L., Erbland, J., Vince, E., Martins, J. M. F., Lerner, B. M., Quinn, P. K., Coffman, D. J., Williams, E. J., and Brown, S. S.: Spatial and diurnal variability in reactive nitrogen oxide chemistry as reflected in the isotopic composition of atmospheric nitrate: Results from the CalNex 2010 field study, Journal of Geophysical Research: Atmospheres, 118, 10,567-10,588, https://doi.org/10.1002/jgrd.50680, 2013.

Vitousek, P. M., Aber, J. D., Howarth, R. W., Likens, G. E., Matson, P. A., Schindler, D. W., Schlesinger, W. H., and Tilman, D. G.: Human Alteration of the Global Nitrogen Cycle: Sources and Consequences, Ecological Applications, 7, 737–750, https://doi.org/10.1890/1051-0761(1997)007[0737:HAOTGN]2.0.CO;2, 1997.

Walters, W. W. and Michalski, G.: Theoretical calculation of nitrogen isotope equilibrium exchange fractionation factors for various NOy molecules, Geochimica et Cosmochimica Acta, 164, 284–297, https://doi.org/10.1016/j.gca.2015.05.029, 2015.

Walters, W. W. and Michalski, G.: Theoretical calculation of oxygen equilibrium isotope fractionation factors involving various NO_y molecules, OH, and H_2O and its implications for isotope variations in atmospheric nitrate, Geochimica et Cosmochimica Acta, 191, 89–101, https://doi.org/10.1016/j.gca.2016.06.039, 2016.

Walters, W. W., Tharp, B. D., Fang, H., Kozak, B. J., and Michalski, G.: Nitrogen isotope composition of thermally produced NO_x from various fossil-fuel combustion sources, Environmental Science & Technology, 49, 11363–11371, https://doi.org/10.1021/acs.est.5b02769, 2015a.

Walters, W. W., Goodwin, S. R., and Michalski, G.: Nitrogen Stable Isotope Composition (δ ^{15} N) of Vehicle-Emitted NO $_x$, Environ. Sci. Technol., 49, 2278–2285, https://doi.org/10.1021/es505580v, 2015b.

Walters, W. W., Simonini, D. S., and Michalski, G.: Nitrogen isotope exchange between NO and NO2 and its implications for δ15N variations in tropospheric NOx and atmospheric nitrate, Geophysical Research Letters, 43, 440–448, https://doi.org/10.1002/2015GL066438, 2016.

https://doi.org/10.5194/egusphere-2023-744
Preprint. Discussion started: 28 April 2023

Walters, W. W., Fang, H., and Michalski, G.: Summertime diurnal variations in the isotopic composition of atmospheric nitrogen dioxide at a small midwestern United States city, Atmospheric Environment, 179, 1–11, https://doi.org/10.1016/j.atmosenv.2018.01.047, 2018.

Wang, Y., Zhang, Q. Q., He, K., Zhang, Q., and Chai, L.: Sulfate-nitrate-ammonium aerosols over China: response to 2000–2015 emission changes of sulfur dioxide, nitrogen oxides, and ammonia, Atmospheric Chemistry and Physics, 13, 2635–2652, https://doi.org/10.5194/acp-13-2635-2013, 2013.

Wang, Y., Gao, W., Wang, S., Song, T., Gong, Z., Ji, D., Wang, L., Liu, Z., Tang, G., Huo, Y., Tian, S., Li, J., Li, M., Yang, Y., Chu, B., Petäjä, T., Kerminen, V.-M., He, H., Hao, J., Kulmala, M., Wang, Y., and Zhang, Y.: Contrasting trends of PM2.5 and surface-ozone concentrations in China from 2013 to 2017, National Science Review, 7, 1331–1339, https://doi.org/10.1093/nsr/nwaa032, 2020.

Wang, Y., Liu, J., Jiang, F., Chen, Z., Wu, L., Zhou, S., Pei, C., Kuang, Y., Cao, F., Zhang, Y., Fan, M., Zheng, J., Li, J., and Zhang, G.: Vertical measurements of stable nitrogen and oxygen isotope composition of fine particulate nitrate aerosol in Guangzhou city: Source apportionment and oxidation pathway, Science of The Total Environment, 865, 161239, https://doi.org/10.1016/j.scitotenv.2022.161239, 2023.

Wang, Y.-L., Song, W., Yang, W., Sun, X.-C., Tong, Y.-D., Wang, X.-M., Liu, C.-Q., Bai, Z.-P., and Liu, X.-Y.: Influences of Atmospheric Pollution on the Contributions of Major Oxidation Pathways to PM2.5 Nitrate Formation in Beijing, Journal of Geophysical Research: Atmospheres, 124, 4174–4185, https://doi.org/10.1029/2019JD030284, 2019.

Wayne, R. P., Barnes, I., Biggs, P., Burrows, J. P., Canosa-Mas, C. E., Hjorth, J., Le Bras, G., Moortgat, G. K., Perner, D., Poulet, G., Restelli, G., and Sidebottom, H.: The nitrate radical: Physics, chemistry, and the atmosphere, Atmospheric Environment. Part A. General Topics, 25, 1–203, https://doi.org/10.1016/0960-1686(91)90192-A, 1991.

Weber, S., Uzu, G., Calas, A., Chevrier, F., Besombes, J.-L., Charron, A., Salameh, D., Ježek, I., Močnik, G., and Jaffrezo, J.-L.: An apportionment method for the oxidative potential of atmospheric particulate matter sources: application to a one-year study in Chamonix, France, Atmospheric Chemistry and Physics, 18, 9617–9629, https://doi.org/10.5194/acp-18-9617-2018, 2018.

Whiteman, C. D.: Breakup of Temperature Inversions in Deep Mountain Valleys: Part I. Observations, Journal of Applied Meteorology and Climatology, 21, 270–289, https://doi.org/10.1175/1520-0450(1982)021<0270:BOTIID>2.0.CO;2, 1982.

WHO: Whorld Health Organization global air quality guidelines: particulate matter (PM2.5 and PM10), ozone, nitrogen dioxide, sulfur dioxide and carbon monoxide, 2021.

Wild, O., Zhu, X., and Prather, M. J.: Fast-J: Accurate simulation of in- and below-cloud photolysis in tropospheric chemical models, Journal of Atmospheric Chemistry, 37, 245–282, https://doi.org/10.1023/A:1006415919030, 2000.

https://doi.org/10.5194/egusphere-2023-744
Preprint. Discussion started: 28 April 2023

Xue, C.: Substantially Growing Interest in the Chemistry of Nitrous Acid (HONO) in China: Current Achievements, Problems, and Future Directions, Environ. Sci. Technol., 56, 7375–7377, https://doi.org/10.1021/acs.est.2c02237, 2022.

Yu, Z. and Elliott, E. M.: Novel Method for Nitrogen Isotopic Analysis of Soil-Emitted Nitric Oxide, Environ. Sci. Technol., 51, 6268–6278, https://doi.org/10.1021/acs.est.7b00592, 2017.

Zhang, L., Vet, R., O'Brien, J. M., Mihele, C., Liang, Z., and Wiebe, A.: Dry deposition of individual nitrogen species at eight Canadian rural sites, Journal of Geophysical Research: Atmospheres, 114, https://doi.org/10.1029/2008JD010640, 2009.

Zhang, R., Wang, G., Guo, S., Zamora, M. L., Ying, Q., Lin, Y., Wang, W., Hu, M., and Wang, Y.: Formation of Urban Fine Particulate Matter, Chem. Rev., 115, 3803–3855, https://doi.org/10.1021/acs.chemrev.5b00067, 2015.

Zhang, W., Bi, X., Zhang, Y., Wu, J., and Feng, Y.: Diesel vehicle emission accounts for the dominate NOx source to atmospheric particulate nitrate in a coastal city: Insights from nitrate dual isotopes of PM2.5, Atmospheric Research, 278, 106328, https://doi.org/10.1016/j.atmosres.2022.106328, 2022a.

Zhang, Y.-L., Zhang, W., Fan, M.-Y., Li, J., Fang, H., Cao, F., Lin, Y.-C., Wilkins, B. P., Liu, X., Bao, M., Hong, Y., and Michalski, G.: A diurnal story of $\Delta^{17}O(NO_3^-)$ in urban Nanjing and its implication for nitrate aerosol formation, npj Clim Atmos Sci, 5, 1–10, https://doi.org/10.1038/s41612-022-00273-3, 2022b.

Zong, Z., Wang, X., Tian, C., Chen, Y., Fang, Y., Zhang, F., Li, C., Sun, J., Li, J., and Zhang, G.: First Assessment of NOx Sources at a Regional Background Site in North China Using Isotopic Analysis Linked with Modeling, Environmental Science and Technology, 51, 5923–5931, https://doi.org/10.1021/acs.est.6b06316, 2017.

Zong, Z., Sun, Z., Xiao, L., Tian, C., Liu, J., Sha, Q., Li, J., Fang, Y., Zheng, J., and Zhang, G.: Insight into the Variability of the Nitrogen Isotope Composition of Vehicular NO_x in China, Environ. Sci. Technol., acs.est.0c04749, https://doi.org/10.1021/acs.est.0c04749, 2020.